



저작자표시-동일조건변경허락 2.0 대한민국

이용자는 아래의 조건을 따르는 경우에 한하여 자유롭게

- 이 저작물을 복제, 배포, 전송, 전시, 공연 및 방송할 수 있습니다.
- 이차적 저작물을 작성할 수 있습니다.
- 이 저작물을 영리 목적으로 이용할 수 있습니다.

다음과 같은 조건을 따라야 합니다:



저작자표시. 귀하는 원저작자를 표시하여야 합니다.



동일조건변경허락. 귀하가 이 저작물을 개작, 변형 또는 가공했을 경우에는, 이 저작물과 동일한 이용허락조건하에서만 배포할 수 있습니다.

- 귀하는, 이 저작물의 재이용이나 배포의 경우, 이 저작물에 적용된 이용허락조건을 명확하게 나타내어야 합니다.
- 저작권자로부터 별도의 허가를 받으면 이러한 조건들은 적용되지 않습니다.

저작권법에 따른 이용자의 권리는 위의 내용에 의하여 영향을 받지 않습니다.

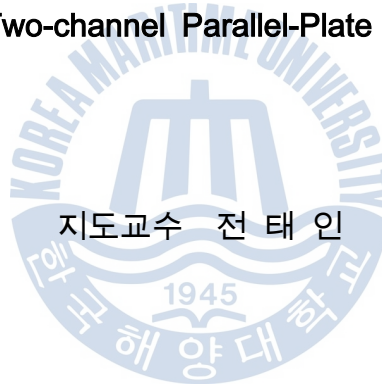
이것은 [이용허락규약\(Legal Code\)](#)을 이해하기 쉽게 요약한 것입니다.

[Disclaimer](#)

공학박사 학위논문

테라헤르츠 평행도파로를 이용한
포토레지스트 박막의 두께 및 길이 변화 측정

Terahertz sensing Photoresist Dependent Thickness and Length
by Using Two-channel Parallel-Plate Waveguides



지도교수 전태인

2015년 01월

한국해양대학교 대학원

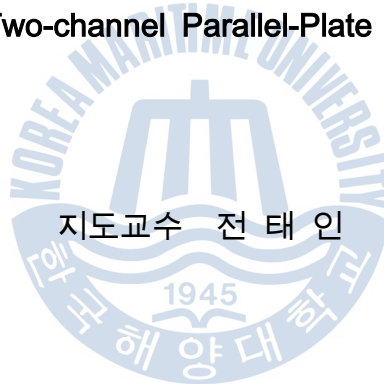
전기전자공학부

박현상

공학박사 학위논문

테라헤르츠 평행도파로를 이용한
포토레지스트 박막의 두께 및 길이 변화 측정

Terahertz sensing Photoresist Dependent Thickness and Length
by Using Two-channel Parallel-Plate Waveguides



지도교수 전태인

2015년 01월

한국해양대학교 대학원

전기전자공학부
박현상

본 논문을 홍길동의 工學碩士 학위논문으로 인준함.



위원장

장 낙 원 (인)

위 원

전 태 인 (인)

위 원

주 양 익 (인)

2015년 01월

한국해양대학교 대학원

PREFACE

I would like to thank my adviser Dr. Tae-In Jeon. He give me chance to study in lab. Luckily, I learn a specialized skill about Terahertz. When the path of learning is long and winding. He show me by doing include his knowledge, wisdom, guidance, patience and passion of study.

I would like to thank my senior Dr. Young-Bin Ji, Eui Su Lee Jeong Sang Jo as well as colleagues Dr. Jingshu Zha, Geun-Ju Kim.

I would like to thank other friend Huk Piri(Ocarina), Sin Myoung (Samulnori), Chamsarang Yahak(night school). because of them I can recover energy and keep it up.

Finally, I would like to thank my parents Hong Suk Bark and soon ok Han and young sister Hyeon Suk Bark. Family is most important supporter in my life.

TABLE OF CONTENTS

Chapter	Page
Chapter 1 Introduction	1
1.1 What is Terahertz?	1
1.2 THz Pulse Generation and Detection	3
1.2.1 THz pulse Genneration	3
1.2.1 THz pulse Detection	5
1.3 Experiment result	7
1.4 Overview of Thesis	8
Chapter 2 Theory	9
2.1 Waveguide Theory : PPWG	9
2.1.1 Mode Classification	9
2.1.2 TE and TM Mode	9
Chapter 3 Finite-Difference Time-Domain (FDTD)	15
3.1 what is FDTD (Finite-Difference Time-Domain)?	15
3.2 1D FDTD	15
3.3 2D FDTD	18
3.3.1 TE Simulation	18
3.3.2 TM Simulation	21

Chapter	Page
Chapter 4 Application 1 : Thin Film sensing	25
4.1 Wave guide : PPWG	25
4.1.1 many kind of Waveguide	25
4.1.2 History of PPWG	27
4.2 What is hin film	28
4.3 Method of thin film sensing	28
4.4 PPWG : Parallel-plate waveguide sensing	30
4.4.1 Simulation condition	30
4.4.2 Simulation : Thin film sensing	32
4.4.3 Experiment Set up & Thin film	41
4.4.4 Experiment : Thin film sensing	46
4.4.5 Analysis	54
Chapter 5 Conclusion	58
5.1 waveguide sensing	58

LIST OF FIGURES

Figure		Page
1.1	Radio wave, a microwave, a terahertz wave, an infrared wave(heat), a light wave, an ultraviolet ray, an X-ray.	1
1.2	Technique of THz pulse generation. (a) photo-conductive antenna : PCA, (b) optical rectification : OR, (c) surface-field of semiconductor	3
1.3	THz pulse generation from a PC with a femto-second optical pulse. propagation of current pulses along the coplanar transmission lines are show in the top view.	3
1.4	Technique of THz pulse measurement. (a) photo-conductive antenna : PCA, (b) electro-optic sampling : EOS.	5
1.5	Terahertz time domain system for coherent emission and detection of THz pulse. THz pulse are mechanically chopped. beam splitter divide short optical pulse, after adding time delay, synchronously gate the detector. Emitted THz pulse is recorded as a function of the delay time.	6
1.6	Measured THz pulsed by using TDS system (red line is humidity 3%, blue line is humidity 48%). (a) time domain THz pulse detected with dipole antennas on LT-GaAs. (b) Fourier-transformed amplitude spectrum of (a).	7
2.1	Schematic diagram of PPWG. z-direction of propagation and d is air gab between two plate.	9
2.2	Dependent TE and TM mode shape in PPWG electric and Magnetic. (a) Transverse Electric modes in PPWG, (b) Transverse Magnetic modes in PPWG.	11
2.3	Cuf off frequency.	12
2.4	Dependent TE and TM mode shape in PPWG electric and Magnetic. (a) Transverse Electric modes in PPWG, (b) Transverse Magnetic modes in PPWG.	13

Figure		Page
2.5	A TE and TM wave reflection off a perfect metal.	14
3.1	The arrangement of electric (circle) and magnetic (rectangular) field nodes in space and time. space time is divided as dot line between future and past values with moving a half temporal step. as difference equation, point (a) is expanded to get an update equation for Hy, point (b) is written to get an update equation for Ex.	16
3.2	Spatial offset between the magnetic and electric fields in 1D FDTD simulation.	17
3.3	Spatial arrangement in 1D FDTD space. x-direction electric and y-direction magnetic field is assumed in the same index	17
3.4	Location of the TE fields in the computational domain.	18
3.5	Location of the TM fields in the computational domain.	21
4.1	Various Waveguide. (a) Parallel-plate Waveguide. (b) Rectangular Waveguide. (c) Circular Waveguide. (d) Two wire lines Waveguide. (e) Single wire line Waveguide.	25
4.2	Schematic waveguide and technique. (a) Improvement of THz coupling using a tapered parallel-plate waveguide, (b) Terahertz band gap properties by using metal slits in tapered parallel-plate Waveguide.	27
4.3	THz thin-film Sensing. (a) Transmission-mode with THz-TDS, (b) Reflection-mode with THz-TDS, (c) Waveguide, (d) Filters and resonators, (e) Metamaterials, (f) Plasmonic structures.	28
4.4	Schematic of 2D FDTD simulation space. (a) air gap is 100 μ m and slit width is 60 μ m, (b) gaussian pulse equation, (c) free space permittivity, (d) dielectric permittivity, (e) Magnetic and electric space in FDTD, (f) thin layer range of length, thickness, refractive index, (g) boundary condition and mesh size, (h) acquiring data line.	30

Figure**Page**

- 4.5 The transmission spectra of the length-dependent resonances, which are 0 to 20 mm in length with a fixed thickness of 1.00 μm and a refractive index of 1.7. Solid lines indicate that the upper channel is open and the lower channel is close. dot lines indicate that the lower channel is open and the upper channel is close. **Insert** : frequency shifts for different film lengths. thin film respectively, for the open upper channel (red triangles) and for the open lower channel (inverse blue triangles). 32
- 4.6 The transmission spectra of the length-dependent resonances, which are 0 to 20 mm in length with a fixed thickness of 1.50 μm and a refractive index of 1.7. Solid lines indicate that the upper channel is open and the lower channel is close. dot lines indicate that the lower channel is open and the upper channel is close. **Insert** : frequency shifts for different film lengths. thin film respectively, for the open upper channel (red triangles) and for the open lower channel (inverse blue triangles). 34
- 4.7 Compared thickness 1.0 μm and 1.5 μm thin film depend on frequency shifts for different thin film lengths. thin film respectively, for the open upper channel (triangles) and for the open lower channel (inverse triangles). thickness 1.50 μm length-dependent frequency shift fitting line (red line), thickness 1.00 μm length-dependent frequency shift fitting line (blue line). 35
- 4.8 The transmission spectra of the thickness-dependent resonances, which are 0 to 20 mm in length with a fixed thickness of 1.50 μm and a refractive index of 1.7. Solid lines indicate that the upper channel is open and the lower channel is close. dot lines indicate that the lower channel is open and the upper channel is close. **Insert** : frequency shifts for different film lengths. thin film respectively, for the open upper channel (red triangles) and for the open lower channel (inverse blue triangles). 37

Figure		Page
4.9	<p>The transmission spectra of the refractive index-dependent resonances shift, which are 1 to 4 refractive index with a fixed thickness of 1.50 μm and a length of 1mm. Solid lines indicate that the upper channel is open and the lower channel is close. Dot lines indicate that the lower channel is open and the upper channel is close. Insert : frequency shifts for different film refractive index. Thin film respectively, for the open upper channel (red triangles) and for the open lower channel (inverse blue triangles).</p>	39
4.10	<p>Schematic diagram of THz time domain system with PPWG between two papabolic mirrors.</p>	41
4.11	<p>The waveguide structure. A single slit sheet is located in the middle of the PPWG air gap to divide the two channels. The front part of the sheet can be bent in an upper or lower direction (indicated by the dashed lines) to open only one of the channels. A thin dielectric layer (SU-8) is on the upper PPWG block surface.</p>	42
4.12	<p>The waveguide structure. (a) Total, Waveguide width and hight length are 63 mm and 172 mm. (b) A single slit sheet is located in the middle of the PPWG and spacer to divide the two channels. aluminum spacer make 100 μm air gab each of channels. metal sheet has single slit which is 60 μm width.</p>	43
4.13	<p>Process, product thickness-dependent thin film samples. Step 1 : Spin coating, drop the PR (photo resistor) on the PPWG controlled speed by using step motor. Step 2 : Soft bake at 150 degrees, 20 Minute to 25 Minute to make hard samples. Be completed thin film on the PPWG easily can measure combined with lower sid of plate like upper picture.</p>	44
4.14	<p>Measured transmission spectra for different film lengths. Lower right insets show the normalized reference spectrum (no coated layer). Lower left insets show the slit sheet bent in a lower or upper direction. (a) The input THz beam travels to the upper channel only. (b) The input THz beam travels to the lower channel only.</p>	46

Figure		Page
4.15	Measured time delay. The red and blue fitting lines indicate the upper and lower channel open only respectively. (a) time delay depend on different film length. (b) time delay of THz pulse.	48
4.16	Measured transmission spectra for different film thickness. Lower right insets show the resonance shift. Lower left insets show the slit sheet bent in a lower or upper direction. (a) The input THz pulse travels to the upper channel only. (b) The input THz pulse travels to the lower channel only.	50
4.17	Comparison of the experimental (blue) and simulated (red). The solid and dashed lines indicate linear fitting for the data. (a) Frequency shifts for different layer lengths. thin film thicknesses used in experimental and simulation conditions are 1.33 ± 0.18 and $1.50 \mu\text{m}$, respectively, for the open upper channel (red triangles) and 1.04 ± 0.08 and $1.00 \mu\text{m}$, respectively, for the open lower channel (inverse blue triangles). (b) Frequency shifts for different thin film thickness. Layer lengths used in experimental and simulation conditions are both 5 mm for the open upper channel (red triangles) and for the open lower channel (inverse blue triangles).	52
4.18	2D FDTD simulation time domain shift and FDTD animation (a) Main pulse and leak out of slit have time difference when input THz pulse travels to the upper channel only, (b) main pulse and leak out of slit have time difference when the input THz pulse travels to the lower channel only.	54
4.19	Measured transmission spectra for different thin film lengths. Blue line is the input THz pulse travels to the upper channel only with 20 mm length of thin film. Red line is the input THz pulse travels to lower channel only with 20 mm length of thin film. black line is Reference (without thin film on PPWG).	56

LIST OF TABLES

Table		Page
1.1	Visible, Infrared and Terahertz Transfer	2
1.2	Characteristics of ultrafast photo-conductive materials	4
4.1	Simulation : Resonance point of length-dependent Thin Film	33
4.2	Simulation : Resonance point of length-dependent Thin Film	35
4.3	Simulation : Resonance point of thickness-dependent thin film	38
4.4	Simulation : Resonance point of refractive index-dependent Thin Film	40
4.5	Thin film thickness depend on speed of motor	45
4.6	Experiment : Resonance point of length-dependent Thin Film	47
4.7	Experiment : Resonance point of thickness-dependent Thin Film	51
4.8	Q-factor	57

► the work presented in this thesis is based on the work published in the following papers in refereed journals :

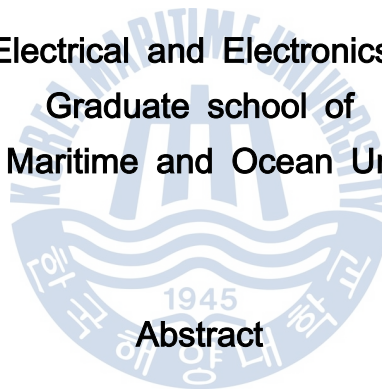
P1 Hyeon Sang Bark,¹ Jingshu Zha,¹ Eui Su Lee,² and Tae-In Jeon, "Thin layer terahertz sensing using two-channel parallel-plate waveguides", Opt Express, 22, 16739 (2014)

Terahertz sensing Photoresist Dependent Thickness and Length
by Using Two-channel Parallel-Plate Waveguides

테라헤르츠 평행도파로를 이용한
포토레지스트 박막의 두께 및 길이 변화 측정

Hyeon Sang Bark

Division of Electrical and Electronics Engineering
Graduate school of
Korea Maritime and Ocean University



Abstract

Key words: THz time-domain spectroscopy, structure II hydrates, thin photoresist film sensing.

본 논문에서 **Chapter 1** 테라헤르츠(Terahertz : 0.1 ~ 10THz)란 무엇인지에 대하여, 다른 종류의 전파 특성과 비교하여 테라파를 서술하였다. 또한 본 논문에서 지금까지 사용되어진 대표적인 테라파 발생과 측정 방식과 원리를 설명하였다. 본 논문에서는 광전도 안테나 PCA (Photoconductive antenna) 방식을 사용하였으며, 테라파 시스템에 대한 설명을 하였다.

평행 도파로를 진행하는 전자기파에 대한 이론을 **Chapter 2**에 서술하였다. 특히, TE (transverse electric) mode 와 TM (transverse magnetic) mode에 대한 이론적인 분석을 통하여 평행도파로 내에서 전파하는 각각의 모드에서의 군속도 분산과 차단 주파수에 대해 서술하였다.

FDTD 시뮬레이션에 대해 **Chapter 3**에 서술하였다. 전기장과 자기장 사이의 맥스웰 방정식을 가상의 공간에서 컴퓨터 계산에 적용하기 위하여, FDTD 시뮬레이션 조건에 대해 설명과, 알고리즘을 적용하여 1차, 2차원의 공간에서의 맥스웰 방정식을 계산 하기위한 방식에 대해 이야기 하고 2차원 공간에서는 전자기파의 대표적인 TE 모드 TM 모드로 나누어 서술하였다.

Chapter 4에서는 평행 도파로를 이용한 박막 측정하였다. 처음으로, **Chapter 4.1 to 4.3**에서는 평행 도파로를 이용한 박막 측정 방식과 지금까지 사용되어진 테라파를 이용한 다양한 측정 방식에 대해 서술하였다. 두 번째로, **Chapter 4.4.2**에서는 **Chapter 3**에서 공부한 FDTD 시뮬레이션을 이용하여 박막의 길이와 두께에 따른 TTS (time turning sensitivity) 와 FTS (frequency turning sensitivity)를 예측하였다. 마지막으로, **Chapter 4.4.5** 실험을 통하여 박막의 두께와 길이를 변화시켜 측정하고 앞의 시뮬레이션과 비교 분석하여 resonance 이동의 원인에 대한 분석을 하였다.

Chapter 1 Introduction

1.1 what is Terahertz wave?

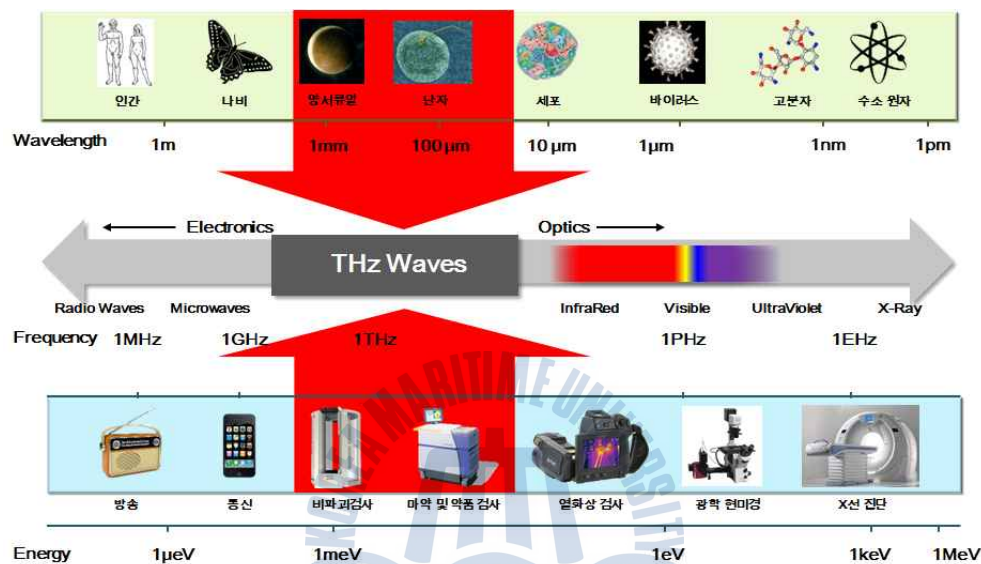


Fig. 1.1 Radio wave, a microwave, a terahertz wave, an infrared wave(heat), a light wave, an ultraviolet ray, an X-ray.

What is Terahertz wave? Electromagnetic wave is all round us. Some of it we can see as light. Some of it we can feel as heat. Some of it we can know that is there when we turn on the radio. All this type of electromagnetic have energy, the wave travel speed of light.

Waves, a radio wave, a microwave, a terahertz wave, an infrared wave (heat), a light wave, an ultraviolet ray and an X-ray from Fig 1.1. What is difference between them. Each every wave have characteristic by frequency and wave length. Frequency is how many time move up and down each second. Wave length is distance form one maximum wave to other. frequency and wave length relate. High frequency, they has short wavelength and low

frequency, they has long wavelength. Difference, those kind of waves are frequency and wavelength. As we go a radio wave to an X-ray frequency from Fig 1.1 is increase but wavelength is decrease.

Fig 1.1 frequency (wave per second) show us kind of parts of the electromagnetic spectrum. we already have good technology to use like radio, microwave, infrared, visible and x-ray. we can generate and detect most easily. but THz wave has no enough technology to use in our life.

In physics, THz wave, also called sub-milimeter wave, T-ray or THz consist of electromagnetic wave. 1 THz mean is 10^{12} Hz, from 300 Giga-hertz to 3 THz in free space. Wavelength of wave in THz band range from 1 mm to 100 μ m. Sometime it is know as the sub-milimeter because of wave begins at a wavelength of one millimeter.

Table 1.1 Visible, Infrared and Terahertz Transfer

Input	Visible	Infrared	Terahertz
Glass	yes	no	no
Paper	no	no	yes
Cardboard	no	no	yes
Foam	no	no	yes
Bandage	no	no	yes

Visible : 360 nm - 820 nm, **Infrared** : 700 nm - 1 mm, **Terahertz** : 1 mm - 300 μ m

THz wave has both side characters duplicity of the microwave and straight of the light wave. Because of double-sided character THz wave. Reflected when wave meet with metal and nonionized form like paper, cardboard, foam and bandage from **Table 1.1**, be penetrated. One of hot point is water block penetration of THz wave. Because of strong abortion of water. Thess are reasons. at present, THz wave is highly favoured in the world.

Even though X-ray should be bad for people's health but THz wave not affected to human body because THz wave has enough lower energy than X-ray. This is good reason to make the best use of THz wave. For example organizational diagnosis, hiding explosive, drug-seeking and etc.

1.2 THz Pulse Generation and Detection

1.2.1 THz pulse Generation

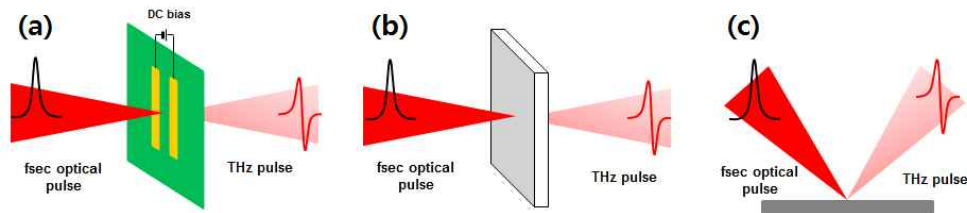


Fig. 1.2 Technique of THz pulse generation. **(a)** photo-conductive antenna : PCA, **(b)** optical rectification : OR, **(c)** surface-field of semiconductor

How we can generate THz Pulse? there are several option, which is Photo-conductive Antenna: PCA [1,2], Optical Rectification : OR, Surface-Field of Semiconductor, to generate THz Pulse.

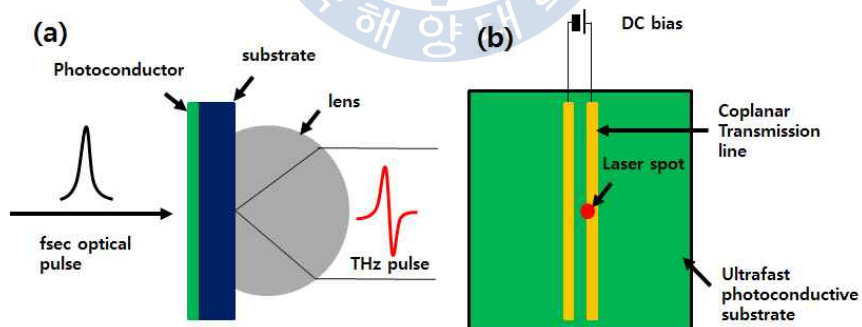


Fig. 1.3 THz pulse generation from a PC with a femto-second optical pulse. propagation of current pulses along the coplanar transmission lines are show in the top view.

This paper chose PCA method to generate THz Pulse. Femto-second pulse focused on the semiconductor strip-line or dipole under DC 5V to 80V. When agitated electron and holes quickly move to biased electrode occurred fast current. Time differential of current is proportional to electromagnetic propagate from antenna to the free space.

PCA has high amplitude and easily adjust output of THz pulse as controlling femto-second pulse power and bias volt. But PCA has limited band width around 0.1 THz to 4.5 THz because of antenna shape and character of semi-conductor of limitation.

Table 1.2 Characteristics of ultrafast photo-conductive materials

Photo-conductive materials	Carrier Lifetime (ps)	Mobility (cm ² / (V·s))	Resistivity (Ω·cm) (Breakdown field, V/cm)	Band gap (eV at R.T.)
SI-GaAs	50-100.0	~1000	10 ⁷	1.43
LT-GaAs	0.3	150 - 200	4 X 10 ⁶ (5 X 10 ⁵)	1.43

SI-GaAs, which is excellent properties as short carrier lifetime, high mobility and high breakdown voltage are needed. **Table 1.2** has information of materials.

1.2.2 Detection

How we can detect THz Pulse? [3] There are several option, which are photo-conductive antenna : PCA and electro-optic sampling : EOS

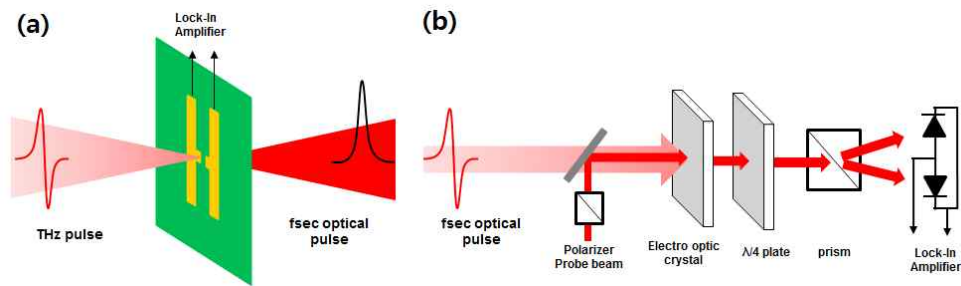


Fig. 1.4 Technique of THz pulse measurement. **(a)** photo-conductive antenna : PCA, **(b)** electro-optic sampling : EOS

The emission of THz pulse is used together in order to explain the detection of a THz pulse. **Fig 1.5** is a standard optical disposition for coherent THz pulse emission and detection.

Ti : sapphire laser is used to generate femto-second pulse. Commonly, laser has short optical pulses with the width ranging from 10 fs to 100 fs at a repetition rate of around 70MHz to 80MHz, depending on the laser system used. THz pulse, mechanically chopped at a few KHz are collimated between two papaboloidal mirror. Sometime, femto-sencond pulse chopped focused on the dipole gap or DC bias electricly chopped is used at a few KHz.

The pumping pulses have photon energy above the direct band-gap of the LT-GaAs. THz pulse is generated with repetition rate as the pumping femto-second optical pulse. Si lens, which is high resistivity hyper-hemispherical (depending on the substrate thickness, collimates generated THz pulse that propagates through the substrate, its refractive index and collimated shape into consideration), affixed closely to the back side of the LT-GaAs source chip.

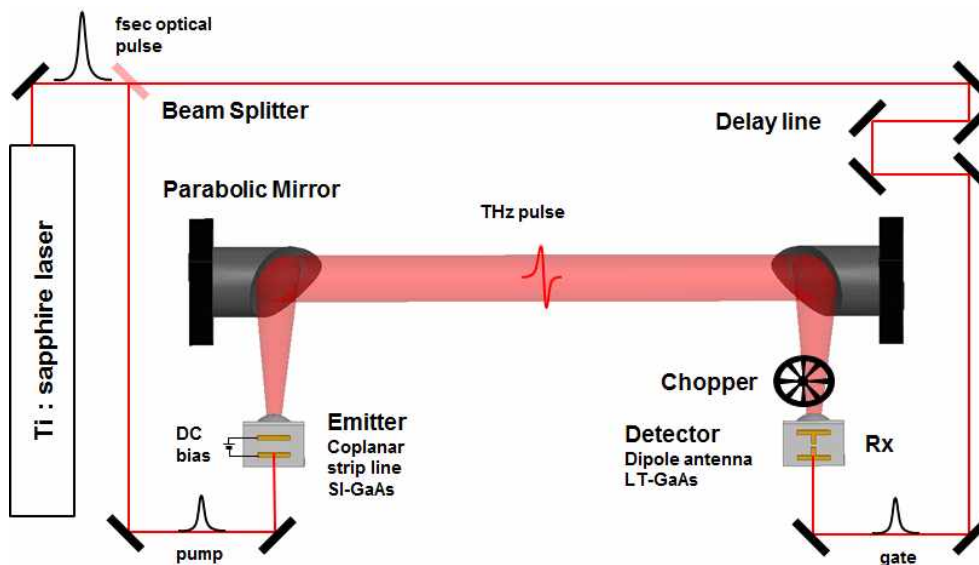


Fig. 1.5 Terahertz time domain system for coherent emission and detection of THz pulse. THz pulse are mechanically chopped. beam splitter divide short optical pulse, after adding time delay, synchronously gate the detector. Emitted THz pulse is recorded as a function of the delay time.

In this system, a symmetric two parabolic mirror and Si lens is used to focus the THz pulse on PC antenna. optical pulses divided by a beam splitter focus on synchronously gate. The PCA detector has 5-10-5 of structure (line width is 5 μm , dipole has 5 μm gab, between line has 10 μm gab). When the carrier lifetime of a PCA is much shorter than the THz pulse, PCA is doing as a sampling gate that samples the waveform of the THz pulse. this detection is called PC sampling. The photo-current measured at the detector, proportional to the electric field of the focused THz pulse, by using low-noise current amplifier and lock-in amplifier. The average photo-current get by moving time delay line between THz pulses and the optical pulse in order to measure THz pulse. A fourier analysis reveals the THz pulse amplitude and phase spectrum [4,5].

1.3 Experiment result

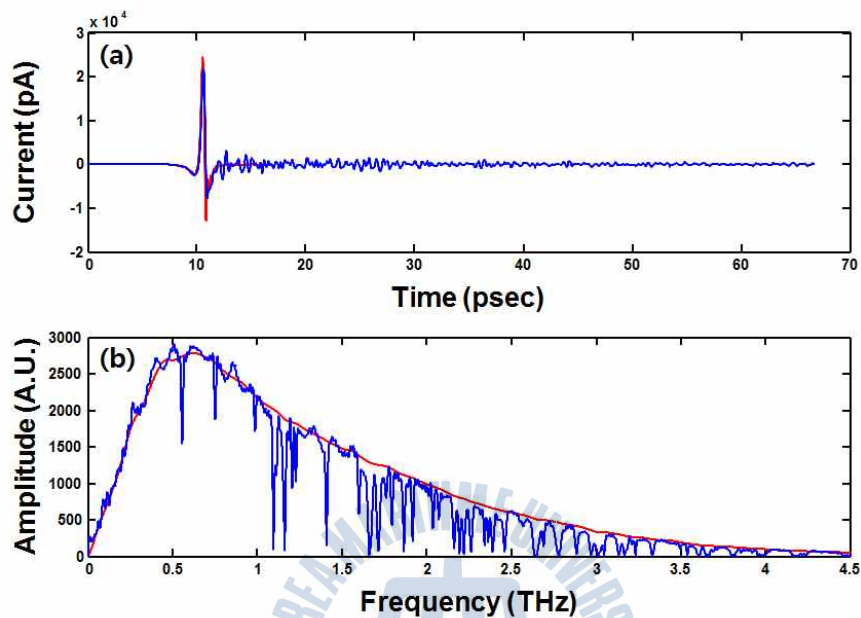


Fig. 1.6 Measured THz pulsed by using TDS system (red line is humidity 3%, blue line is humidity 48%). **(a)** time domain THz pulse detected with dipole antennas on LT-GaAs. **(b)** Fourier-transformed amplitude spectrum of (a).

Fig 1.6 detection show an experimental result with a 10-80-10 structure (line width is 10 μm , between line gab is 80 μm) on SI-GaAs as the emitter and a 5-10-5 structure (line width is 5 μm , dipole has 5 μm gab, between line has 10 μm gab) dipole on LT-GaAs as the detector. The optical pulse having a pulse width of 60 fs at 800 nm and a repetition rate of 80 MHz focus on both the emitter and the detector. This pulse width and the antenna structure has the about 4.5 THz bandwidth.

1.4 Overview of Thesis

Chapter 1 explained what is THz wave and defined THz wave compare with other wave. **Chapter 1, 2** contained general THz generation and detection. especially, this paper is used PCA (Photoconductive antenna) explain system.

Chapter 2 has propagation of wave in the PPWG. especially, TE (transverse electric) mode and TM (transverse magnetic) mode. each of mode try to understand mode dispersion and cut off frequency in the PPWG.

Chapter 3 has principal of FDTD simulation. Frist, relation between electric and magnetic from Maxwell equation simply is writing down how could it changed to C language at 1 Dimension. than, 2 Dimension discuss with propagation of TE and TM mode in the FDTD space.

Chapter 4 has thin film sensing by using PPWG. First, **Chapter 4.1 to 4.3** write down PPWG technique and different thin film measurement. Second, **Chapter 4.4.2** predict thin layer TTS (time turning sensitivity) and FTS (frequency turning sensitivity) by using FDTD simulation. Finally, **Chapter 4.4.5** compare with thin film and experiment dependent-length and -thickness. we analysis principal of resonance and shifting.

Chapter 2 Theory

2.1 Waveguide Theory [PPWG] [6]

2.1.1 Mode Classification

- **TEM waves** : waves do not have electric or magnetic field in the direction of propagation. Plane waves is common example.

- **TM waves [Transverse Magnetic Wave]** : Wave have an electric field but do not have magnetic field in the direction of propagation. Sometime TM is referred to as E waves

- **TE waves [Transverse Electric Wave]** : waves with a magnetic field but do not have electric field in the direction of propagation. Sometime TE is referred to as H waves

Mode Independence, Propagation Constants, and Cutoff Frequencies

2.1.1 Mode

1) Basic Wave Equation

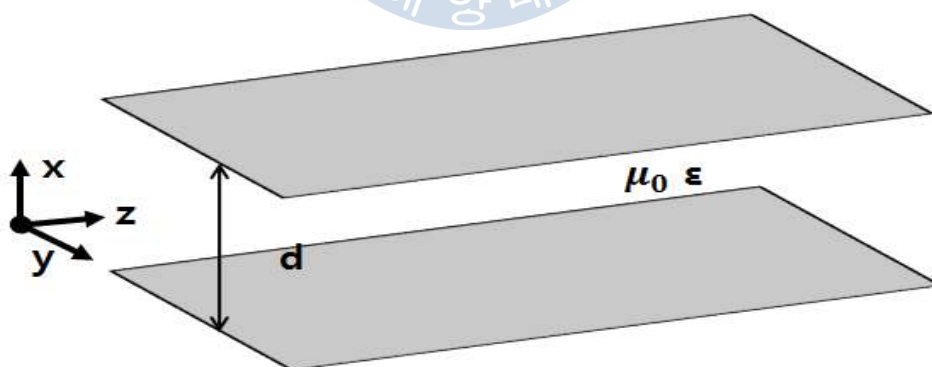


Fig. 2.1 Schematic diagram of PPWG. z-direction of propagation and d is air gap between two plate.

Basic wave equation

$$\nabla^2 E + \omega^2 \mu \varepsilon E = 0$$

$$\frac{\partial^2 E_x}{\partial x^2} + \frac{\partial^2 E_x}{\partial y^2} + \frac{\partial^2 E_x}{\partial z^2} = -\omega^2 \mu \varepsilon E_x$$

$$\frac{\partial^2 E_y}{\partial x^2} + \frac{\partial^2 E_y}{\partial y^2} + \frac{\partial^2 E_y}{\partial z^2} = -\omega^2 \mu \varepsilon E_y$$

$$\frac{\partial^2 E_z}{\partial x^2} + \frac{\partial^2 E_z}{\partial y^2} + \frac{\partial^2 E_z}{\partial z^2} = -\omega^2 \mu \varepsilon E_z$$

$$\nabla^2 H + \omega^2 \mu \varepsilon H = 0$$

$$\frac{\partial^2 H_x}{\partial x^2} + \frac{\partial^2 H_x}{\partial y^2} + \frac{\partial^2 H_x}{\partial z^2} = -\omega^2 \mu \varepsilon H_x$$

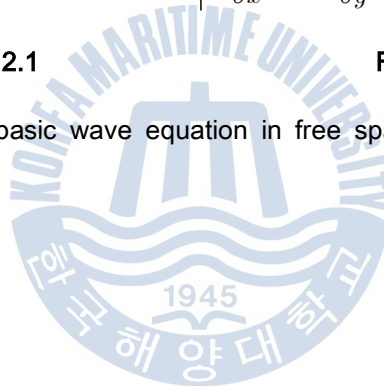
$$\frac{\partial^2 H_y}{\partial x^2} + \frac{\partial^2 H_y}{\partial y^2} + \frac{\partial^2 H_y}{\partial z^2} = -\omega^2 \mu \varepsilon H_y$$

$$\frac{\partial^2 H_z}{\partial x^2} + \frac{\partial^2 H_z}{\partial y^2} + \frac{\partial^2 H_z}{\partial z^2} = -\omega^2 \mu \varepsilon H_z$$

Formula 2.1

Formula 2.2

Formula 2.1, 2.2 is basic wave equation in free space include all direction of wave.



2) TE / TM mode Wave Equation

Transverse Electric (TE) Modes

$$\frac{\partial}{\partial y} = 0 \quad \frac{\partial}{\partial z} \neq 0 \quad \frac{\partial}{\partial x} \neq 0$$

$$\frac{\partial^2 E_y}{\partial x^2} + \frac{\partial^2 E_y}{\partial z^2} = -\omega^2 \mu \epsilon E_y$$

Formula 2.3

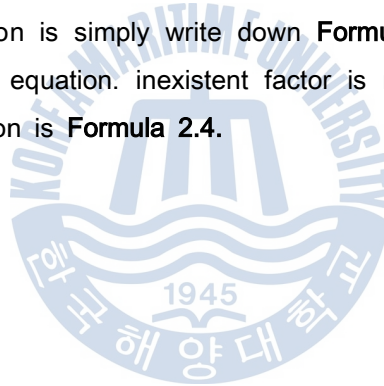
Transverse magnetic (TM) modes

$$\frac{\partial}{\partial y} = 0 \quad \frac{\partial}{\partial x} \neq 0 \quad \frac{\partial}{\partial z} \neq 0$$

$$\frac{\partial^2 H_y}{\partial x^2} + \frac{\partial^2 H_y}{\partial z^2} = -\omega^2 \mu \epsilon H_y$$

Formula 2.4

In Parallel-plate waveguide, the plates are infinite in the y-extent; we consider about propagation in the z-direction. The following TE mode has only H_y in the wave equation. inexistant factor is removed from **Formula 2.1**. TE mode equation is simply write down **Formula 2.3**. TM mode has only E_y in the wave equation. inexistant factor is removed from **Formula 2.2**. TM mode equation is **Formula 2.4**.



3) TE and TM mode

Transverse Electric (TE) Modes

Transverse magnetic (TM) modes

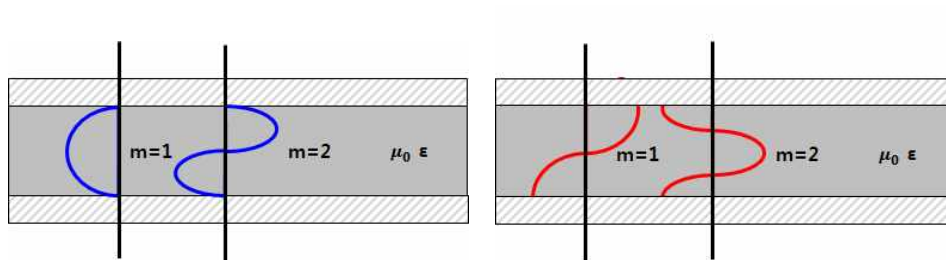


Fig. 2.2 Dependent TE and TM mode shape in PPWG electric and Magnetic. **(a)** Transverse Electric modes in PPWG, **(b)** Transverse Magnetic modes in PPWG.

Transverse Electric (TE) Modes

Transverse magnetic (TM) modes

$E_y(x, z) = e^{-j\beta_z z} [Ae^{-j\beta_x x} + Be^{-j\beta_x x}]$ $F(x) = [Ae^{-j\beta_x x} + Be^{-j\beta_x x}]$ $E_y(x, z) = F(x)e^{-j\beta_z z}$ $-\frac{\partial^2 F(x)}{\partial x^2} = (\omega^2 \mu \epsilon - \beta_z^2)F(x)$ $F(x=0) = F(x=a) = 0$ $F(x) = E_0 \sin(\beta_x x)$ $E_y(x, z) = E_0 e^{-j\beta_z z} \sin \beta_x a$	$H_y(x, z) = e^{-j\beta_z z} [Ae^{-j\beta_x x} + Be^{-j\beta_x x}]$ $G(x) = [Ae^{-j\beta_x x} + Be^{-j\beta_x x}]$ $H_y(x, z) = G(x)e^{-j\beta_z z}$ $-\frac{\partial^2 G(x)}{\partial x^2} = (\omega^2 \mu \epsilon - \beta_z^2)G(x)$ $G(x=0) = G(x=a) = 0$ $G(x) = H_0 \cos(\beta_x x)$ $H_y(x, z) = H_0 e^{-j\beta_z z} \cos \beta_x a = 0$
--	--

Formula 2.5

Formula 2.6

TE and TM wave equation from **Formula 2.3, 2.4**. TE mode electric and TM magnetic equation. Reduce a differential equation by using assumed forward traveling wave equation. From **Formula 2.5, 2.6** replacement $F(x)$ and $G(x)$ should be sine and cosine. Boundary condition leads to y-direction electric and magnetic from TE and TM mode.

4) Mode - Dispersion

Transverse Electric (TE) Modes

$$E_y(x, z) = E_0 \sin\left(\frac{m\pi}{a}x\right)e^{-j\beta_z z} \quad 1$$

$$-\frac{\partial^2 F(x)}{\partial x^2} = (\omega^2 \mu \epsilon - \beta_z^2)F(x) \quad 2$$

$$\beta_z^2 + \beta_x^2 = \omega^2 \mu \epsilon = \beta^2 \quad 3$$

$$\beta_z = \sqrt{\omega^2 \mu \epsilon - \left(\frac{m\pi}{z}\right)^2} \quad 4$$

Formula 2.7

Transverse magnetic (TM) modes

$$H_y(x, z) = H_0 \cos\left(\frac{m\pi}{a}x\right)e^{-j\beta_z z}$$

$$-\frac{\partial^2 G(x)}{\partial x^2} = (\omega^2 \mu \epsilon - \beta_z^2)G(x)$$

$$\beta_z^2 + \beta_x^2 = \omega^2 \mu \epsilon = \beta^2$$

$$\beta_z = \sqrt{\omega^2 \mu \epsilon - \left(\frac{m\pi}{z}\right)^2}$$

Formula 2.8

Formula 2.5, 2.6 lead to wave vector. Dispersion of z-direction easily can get from Formula 2.7, 2.8, respectively. It is called dispersion. Different "m" values correspond to different TE and TM modes.

5) Mode - Cut off Frequency

Transverse Electric (TE) and magnetic (TM) modes

$$\beta_z = \sqrt{\omega^2 \mu \epsilon - \left(\frac{m\pi}{z}\right)^2}$$

$$f > \frac{m}{2a\sqrt{\mu\epsilon}}, \quad \omega^2 \mu \epsilon > \left(\frac{m\pi}{a}\right)^2$$

$$f_c = \frac{m}{2a\sqrt{\mu\epsilon}}, \quad \omega_c = \frac{1}{\sqrt{\mu\epsilon}} \left(\frac{m\pi}{d}\right)$$

Formula 2.9

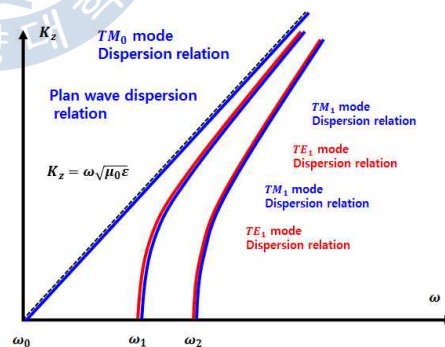


Fig. 2.3 Cuf off frequency.

Formula 2.9 show us Dispersion with TE and TM modes, if the frequency ω is less than then k_z becomes entirely imaginary and the mode does not propagate. This is Cut off Frequency from TE and TM mode.

6) TE magnetic Field and TM electric field

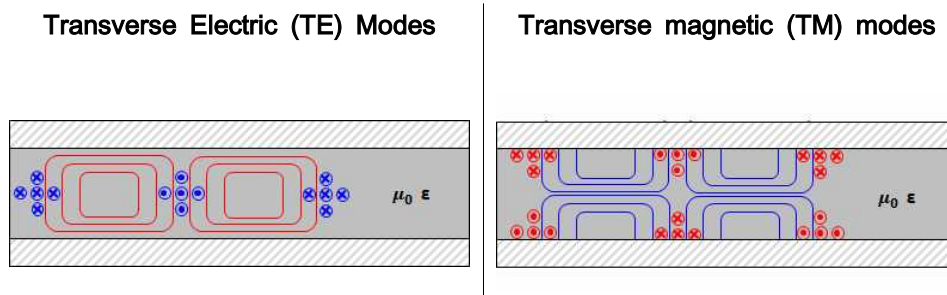


Fig. 2.4 Dependent TE and TM mode shape in PPWG electric and Magnetic. **(a)** Transverse Electric modes in PPWG, **(b)** Transverse Magnetic modes in PPWG.

TE Magnetic	TM Electric
$\nabla \times E = -j\omega\mu H$ $H = \frac{-1}{j\omega\mu} \begin{vmatrix} \vec{x} & \vec{y} & \vec{z} \\ \frac{\partial}{\partial x} & 0 & \frac{\partial}{\partial z} \\ 0 & E_y & 0 \end{vmatrix}$ $H_x(x,z) = \frac{\beta_x}{\omega\epsilon} E_0 e^{-j\beta_z z} [Ae^{-j\beta_x x} + Be^{-j\beta_x x}]$ $H_z(x,z) = -\frac{\beta_x}{\omega\epsilon} E_0 e^{-j\beta_z z} [Ae^{-j\beta_x x} - Be^{-j\beta_x x}]$ $H_x = -\frac{\beta_z}{\omega\mu} E_0 e^{-j\beta_z z} \sin\beta_x x$ $H_z = +\frac{j\beta_x}{\omega\mu} E_0 e^{-j\beta_z z} \cos\beta_x x$ $H = \frac{jE_0}{\omega\mu} \left[\frac{m\pi}{a} \cos\left(\frac{m\pi}{a} z\right) + j \frac{m\pi}{a} \sin\left(\frac{m\pi}{a} x\right) \right] e^{-j\beta_z z}$ <p>$m = 1,2,3,$</p>	$\nabla \times H = j\omega\epsilon E$ $E = \frac{1}{j\omega\epsilon} \begin{vmatrix} \vec{x} & \vec{y} & \vec{z} \\ \frac{\partial}{\partial x} & 0 & \frac{\partial}{\partial z} \\ 0 & H_y & 0 \end{vmatrix}$ $E_x(x,z) = \frac{\beta_x}{\omega\epsilon} H_0 e^{-j\beta_z z} [Ae^{-j\beta_x x} + Be^{-j\beta_x x}]$ $E_z(x,z) = -\frac{\beta_x}{\omega\epsilon} H_0 e^{-j\beta_z z} [Ae^{-j\beta_x x} - Be^{-j\beta_x x}]$ $E_x(x,z) = \frac{\beta_x}{\omega\epsilon} H_0 e^{-j\beta_z z} \cos\beta_x x$ $E_z(x,z) = \frac{j\beta_x}{\omega\epsilon} H_0 e^{-j\beta_z z} \sin\beta_x x$ $E = -\frac{jH_0}{\omega\epsilon} \left[-\frac{m\pi}{a} \sin\left(\frac{m\pi}{a} z\right) + j \frac{m\pi}{a} \cos\left(\frac{m\pi}{a} x\right) \right] e^{-j\beta_z z}$ <p>$m = 1,2,3,$</p>

Formula 2.10

Formula 2.11

Faraday's law lead to magnetic in TE mode H_z and H_x . Ampere' law lead to electric in TM mode E_z and E_x , respectively.

6) Reflection off a perfect metal

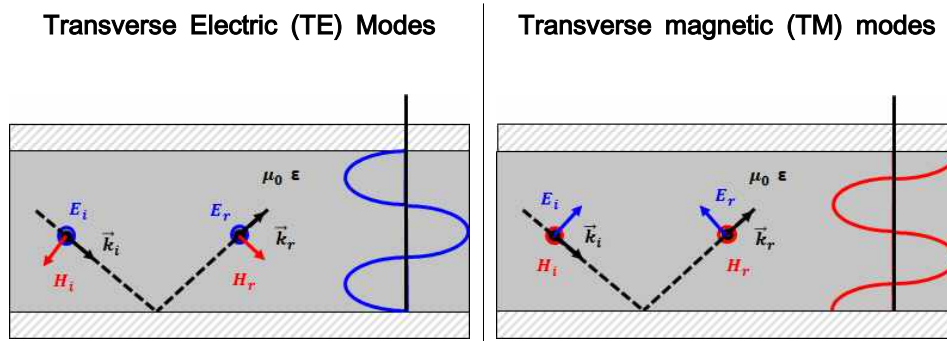


Fig. 2.5 A TE and TM wave reflection off a perfect metal.

TE wave

$$\vec{\beta}_i = \beta_x \vec{x} + \beta_z \vec{z}, \quad \vec{\beta}_r = \beta_x \vec{x} + \beta_z \vec{z}$$

$$E = E_i e^{-j(-\beta_x x + \beta_z z)} + \Gamma E_i e^{-j(\beta_x x + \beta_z z)}$$

$$E = E_i [e^{-j(-\beta_x x + \beta_z z)} - e^{-j(\beta_x x + \beta_z z)}]$$

$$E = 2j E_i \sin(\beta_x x) e^{-j\beta_z z}$$

Formula 2.12

TM wave

$$\vec{\beta}_i = \beta_x \vec{x} + \beta_z \vec{z}, \quad \vec{\beta}_r = \beta_x \vec{x} + \beta_z \vec{z}$$

$$H = H_i e^{-j(-\beta_x x + \beta_z z)} + \Gamma H_i e^{-j(\beta_x x + \beta_z z)}$$

$$H = H_i [e^{-j(-\beta_x x + \beta_z z)} + e^{-j(\beta_x x + \beta_z z)}]$$

$$H = 2 H_i \cos(\beta_x x) e^{-j\beta_z z}$$

Formula 2.13

Formula 2.12, 2.13 show when reflection off a perfect metal. If another top metal plate is placed at the nodes of the "sine" function in TE mode and at the maximum points of the "cosine" function in TM mode then this additional metal plate will not disturb the field. TE and TM waves bouncing back and forth between two metal plates and propagating in the z-direction.

Chapter 3

Finite-Difference Time-Domain (FDTD)

3.1 FDTD [7,8]

Finite-difference time-domain (FDTD) is a numerical analysis technique used for modeling computational electrodynamics. This paper approached numerical solution of the time-dependent Maxwell's curl equations. assumption are z-direction propagation and infinite y-direction. Component of $\partial/\partial y$ derivatives remove from Maxwell's equations (TE, TM independent equations).

3.2 1D FDTD

A one-dimensional space where there are only variations in the z direction. Assume that electric field only has a x component in thin case Faraday's law and Ampere's law can be written

$$-\mu \frac{\partial H}{\partial t} = \nabla \times E = \begin{vmatrix} \hat{a}_x & \hat{a}_y & \hat{a}_z \\ 0 & 0 & \frac{\partial}{\partial z} \\ E_x & 0 & 0 \end{vmatrix} = -\hat{a}_y \frac{\partial E_x}{\partial z} \quad \left| \quad \varepsilon \frac{\partial E}{\partial t} = \nabla \times H = \begin{vmatrix} \hat{a}_x & \hat{a}_y & \hat{a}_z \\ 0 & 0 & \frac{\partial}{\partial z} \\ 0 & H_y & 0 \end{vmatrix} = \hat{a}_x \frac{\partial H_y}{\partial z} \right.$$

Formula 3.1

$$\mu \frac{\partial H_y}{\partial t} = \frac{\partial E_x}{\partial z} \quad \left| \quad \varepsilon \frac{\partial E_x}{\partial t} = \frac{\partial H_y}{\partial z} \right. \begin{matrix} \uparrow x \\ \leftarrow z \end{matrix}$$

Formula 3.2

To replace the derivatives in **Formula 3.2**, discretized space and time will be used to indicate the location where fields are sampled in space and time from **Formula 3.2**.

$$\begin{aligned} E_x(z, t) &= E_x(i \Delta_z, n \Delta_t) = E_x^n [i] \\ H_y(z, t) &= H_y(i \Delta_z, n \Delta_t) = H_y^n [i] \end{aligned}$$

Formula 3.3

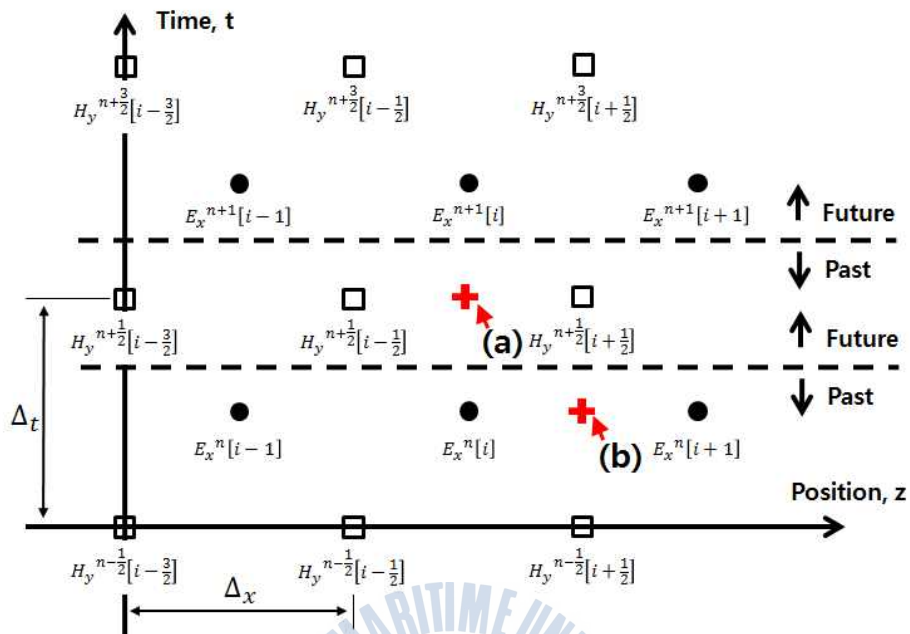


Fig. 3.1. The arrangement of electric (circle) and magnetic (rectangular) field nodes in space and time. Space time is divided as dot line between future and past values with moving a half temporal step. as difference equation, point **(a)** is expanded to get an update equation for H_y , point **(b)** is written to get an update equation for E_x .

Fig 3.1 (a) is replacing the temporal derivative on the left with a finite difference involving $E_x^{n+1}[i]$ and $E_x^n[i]$ and replacing the spatial derivative on the right with a finite difference involving $H_y^{n+\frac{1}{2}}\left[i+\frac{1}{2}\right]$ and $H_y^{n+\frac{1}{2}}\left[i-\frac{1}{2}\right]$ field. **Fig 3.1 (b)** is replacing the temporal derivative on the left with a finite difference involving $E_x^n[i+1]$ and $E_x^n[i]$ and replacing the spatial derivative on the right with a finite difference involving $H_y^{n+\frac{1}{2}}\left[i+\frac{1}{2}\right]$ and $H_y^{n-\frac{1}{2}}\left[i+\frac{1}{2}\right]$ field.

Faraday's law at the space-time point $\left(\left(i + \frac{1}{2} \right) \Delta_x, n \Delta_t \right)$

$$H_y^{n+\frac{1}{2}} \left(i + \frac{1}{2} \right) = H_y^{n-\frac{1}{2}} \left(i + \frac{1}{2} \right) + \frac{\Delta_t}{\mu \Delta_x} (E_z^n(i+1) - E_z^n(i)) \quad \text{Formula 3.4}$$

Ampere's law at the space-time point $\left(i \Delta_x, \left(n + \frac{1}{2} \right) \Delta_t \right)$

$$E_x^{n+1}(i) = E_x^n(i) + \frac{\Delta_t}{\epsilon \Delta_z} \left(H_y^{n+\frac{1}{2}} \left(i + \frac{1}{2} \right) - H_y^{n+\frac{1}{2}} \left(i - \frac{1}{2} \right) \right) \quad \text{Formula 3.5}$$

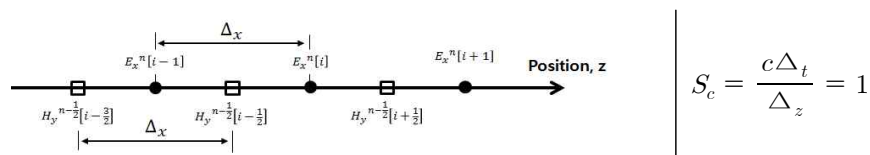


Fig. 3.2 Spatial offset between the magnetic and electric fields in 1D FDTD simulation.

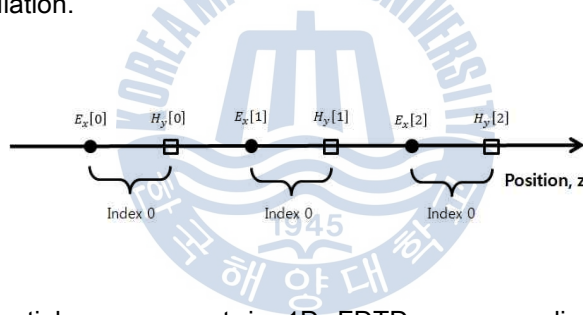


Fig. 3.3 Spatial arrangement in 1D FDTD space. x-direction electric and y-direction magnetic field is assumed in the same index

The temporal offset between the electric and magnetic field is always understood whether explicitly shown from Fig 3.2. Magnetic and electric field is written as computer implementation of a 1D FDTD simulation. Magnetic-field nodes the update equation can be written by $hy[i] = hy[i] + (ez[i + 1] - ez[i]) / imp0$, electric-field nodes the update equation can be written by $ez[i] = ez[i] + (hy[i] - hy[i - 1]) * imp0$.

3.3 2D FDTD

3.1.1 TE mode simulation

Formula 3.6 come from Faraday's law and Ampere' law.

$$-\sigma_m H - \mu \frac{\partial H}{\partial t} = \nabla \times E = \begin{vmatrix} \hat{a}_x & \hat{a}_y & \hat{a}_z \\ \frac{\partial}{\partial x} & 0 & \frac{\partial}{\partial z} \\ 0 & E_y & 0 \end{vmatrix} = \hat{a}_z \frac{\partial E_y}{\partial x} - \hat{a}_x \frac{\partial E_y}{\partial z} \quad \sigma E + \epsilon \frac{\partial E}{\partial t} = \nabla \times H = \begin{vmatrix} \hat{a}_x & \hat{a}_y & \hat{a}_z \\ \frac{\partial}{\partial x} & 0 & \frac{\partial}{\partial z} \\ H_x & 0 & H_z \end{vmatrix} = \hat{a}_y \left(\frac{\partial H_x}{\partial z} - \frac{\partial H_z}{\partial x} \right)$$

Formula 3.6

In the 2 Dimension TE wave (Transverse Electric Wave) mode propagation in z direction. E_y , H_x , E_y , H_z – nonzero components, propagation along z, transverse field variations along x) in lossless media, Maxwell's equations take the following

$$-\sigma_m H_z - \mu \frac{\partial H_z}{\partial t} = \frac{\partial E_y}{\partial x}, \quad \sigma_m H_x - \mu \frac{\partial H_x}{\partial t} = \frac{\partial E_y}{\partial z}, \quad \sigma E_y + \epsilon \frac{\partial E_y}{\partial t} = \frac{\partial H_x}{\partial z} - \frac{\partial H_z}{\partial x}$$

Formula 3.7

Electric and magnetic field are represented by a 2D array Fig 3.4, 3.5 with 2D mesh. Number of space steps account as i (x-direction) and k (z-direction).

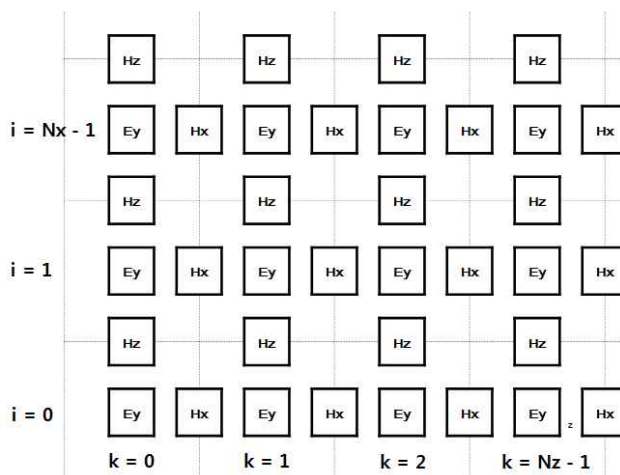


Fig. 3.4 Location of the TE fields in the computational domain.

The TE fields stencil is going to explain as Formula 6 to 12. The Ey field locations coincide with the mesh nodes (i, k) given in 2D computational domain. Each center of grid box represent the FDTD space cell given In **Fig 3.4**. The magnetic fields Hx and Hz are related with cell edges. The electric fields (Ey) are related with integer values of the indices i and k. The magnetic field (x-direction Hx) is related with integer i and (k + 0.5) indices. The magnetic field (z-direction Hz) is associated with (i + 0.5) and integer k indices. The TE mode algorithm can be presented in **Formula 3.8, 3.9**.

The update equation for the z-direction and x-direction of the magnetic field are written by **Formula 3.8** with space-time point $\left(\left(m + \frac{1}{2}\right)\Delta_x, n\Delta_y, q\Delta_t\right)$ and **Formula 3.8** with space-time point $\left(\left(m + \frac{1}{2}\right)\Delta_x, n\Delta_y, q\Delta_t\right)$.

$$H_z^{n+\frac{1}{2}}\left[i, k + \frac{1}{2}\right] = \frac{1 - \frac{\sigma_m \Delta_t}{2\mu}}{1 + \frac{\sigma_m \Delta_t}{2\mu}} H_z^{n-\frac{1}{2}}\left[i, k + \frac{1}{2}\right] - \frac{1}{1 + \frac{\sigma_m \Delta_t}{2\mu}} \frac{\Delta_t}{\mu \Delta_x} (E_y^n[i, k+1] - E_y^n[i, k])$$

$$H_x^{n+\frac{1}{2}}\left[i + \frac{1}{2}, k\right] = \frac{1 - \frac{\sigma_m \Delta_t}{2\mu}}{1 + \frac{\sigma_m \Delta_t}{2\mu}} H_x^{n-\frac{1}{2}}\left[i + \frac{1}{2}, k\right] - \frac{1}{1 + \frac{\sigma_m \Delta_t}{2\mu}} \frac{\Delta_t}{\mu \Delta_z} (E_y^n[i+1, k] - E_y^n[i, k])$$

Formula 3.8

The electric-field update equation is obtained via the finite-difference approximation of **Formula 3.9** expanded about $\left(m\Delta_x, n\Delta_y, \left(q + \frac{1}{2}\right)\Delta_t\right)$

$$E_y^{n+1}[i, k] = \frac{1 - \frac{\sigma \Delta_t}{2\epsilon}}{1 + \frac{\sigma \Delta_t}{2\epsilon}} E_y^n[i, k] + \frac{1}{1 + \frac{\sigma \Delta_t}{2\epsilon}} \left(\frac{\Delta_t}{\epsilon \Delta_z} \left\{ H_x^{n+\frac{1}{2}}\left[i + \frac{1}{2}, k\right] - H_x^{n+\frac{1}{2}}\left[i - \frac{1}{2}, k\right] \right\} \right. \\ \left. - \frac{\Delta_t}{\epsilon \Delta_x} \left\{ H_z^{q+\frac{1}{2}}\left[m, n + \frac{1}{2}\right] - H_z^{q+\frac{1}{2}}\left[m, n - \frac{1}{2}\right] \right\} \right)$$

Formula 3.9

There quantities from **Formula 3.10** simply appear in the update equations and employ the following naming convention to C language.

$$\begin{aligned}
 C_{hzh}\left(i, k + \frac{1}{2}\right) &= \frac{1 - \frac{\sigma_m \Delta_t}{2\mu}}{1 + \frac{\sigma_m \Delta_t}{2\mu}} \Bigg|_{i\Delta_z, \left(i + \frac{1}{2}\right)\Delta_z} & C_{hze}\left(i, k + \frac{1}{2}\right) &= \frac{1}{1 + \frac{\sigma \Delta_t}{2\mu}} \frac{\Delta_t}{\mu \delta} \Bigg|_{i\Delta_z, \left(i + \frac{1}{2}\right)\Delta_z} \\
 C_{exe}\left(i + \frac{1}{2}, k\right) &= \frac{1 - \frac{\sigma_m \Delta_t}{2\mu}}{1 + \frac{\sigma_m \Delta_t}{2\mu}} \Bigg|_{\left(i + \frac{1}{2}\right)\Delta_z, k\Delta_z} & C_{exh}\left(i + \frac{1}{2}, k\right) &= \frac{1}{1 + \frac{\sigma \Delta_t}{2\mu}} \frac{\Delta_t}{\mu \delta} \Bigg|_{\left(i + \frac{1}{2}\right)\Delta_z, k\Delta_z} \\
 C_{eye}(i, k) &= \frac{1 - \frac{\sigma_m \Delta_t}{2\varepsilon}}{1 + \frac{\sigma_m \Delta_t}{2\varepsilon}} \Bigg|_{i\Delta_z, k\Delta_z} & C_{eyh}\left(i, k + \frac{1}{2}\right) &= \frac{1}{1 + \frac{\sigma \Delta_t}{2\varepsilon}} \frac{\Delta_t}{\varepsilon \delta} \Bigg|_{i\Delta_z, k\Delta_z}
 \end{aligned}$$

Formula 3.10

These equations translate suitable computer program with C language. Following **Chapter 3.2** approach that was used in one dimension. Form as illustrated in Fig 3.4, an Hx node is assumed to be a half spatial step further in the z direction than the corresponding Ey node with the same indices. Similarly, an Hz node is assumed to be a half spatial step further in the x direction than the corresponding Ey node with the same indices. Finally, Translated TE mode is written by

$$\begin{aligned}
 H_z(i, k) &= Chxh(i, k) * H_z(i, k) - Chxe(i, k) * (Ey(i, k + 1) - Ey(i, k)); \\
 H_x(i, k) &= Chyh(i, k) * H_x(i, k) + Chye(i, k) * (Ex(i + 1, k) - Ex(i, k)); \\
 E_y(i, k) &= Ceze(i, k) * E_y(i, k) + \\
 &\quad Cezh(i, k) * ((H_x(i, k) - H_x(i - 1, k)) - (H_z(i, k) - H_z(i, k - 1)));
 \end{aligned}$$

Formula 3.11

3.1.2 TM mode simulation

Formula 3.12 come from Faraday's law and Ampere' law.

$$\sigma E + \varepsilon \frac{\partial E}{\partial t} = \nabla \times H = \begin{bmatrix} \hat{a}_x & \hat{a}_y & \hat{a}_z \\ \frac{\partial}{\partial x} & 0 & \frac{\partial}{\partial z} \\ 0 & H_y & 0 \end{bmatrix} = \hat{a}_z \frac{\partial H_y}{\partial x} - \hat{a}_x \frac{\partial H_y}{\partial z} \quad -\sigma_m H - \mu \frac{\partial H}{\partial t} = \nabla \times E = \begin{bmatrix} \hat{a}_x & \hat{a}_y & \hat{a}_z \\ \frac{\partial}{\partial x} & 0 & \frac{\partial}{\partial z} \\ E_x & 0 & E_z \end{bmatrix} = \hat{a}_y \left(\frac{\partial E_x}{\partial z} - \frac{\partial E_z}{\partial x} \right)$$

Formula 3.12

In the 2D TM case (E_x , H_y , E_z — nonzero components, propagation along Z, transverse field variations along X) in lossless media, Maxwell's equations take the following form

$$\sigma E_z + \varepsilon \frac{\partial E_z}{\partial t} = \frac{\partial H_y}{\partial x}, \quad \sigma E_x + \varepsilon \frac{\partial E_x}{\partial t} = \frac{\partial H_y}{\partial z}, \quad -\sigma_m H_y - \mu \frac{\partial H_y}{\partial t} = \frac{\partial E_x}{\partial z} - \frac{\partial E_z}{\partial x}$$

Formula 3.13

The location of the TM fields in the computational domain follows the same philosophy and is shown in **Figure 3.5**.

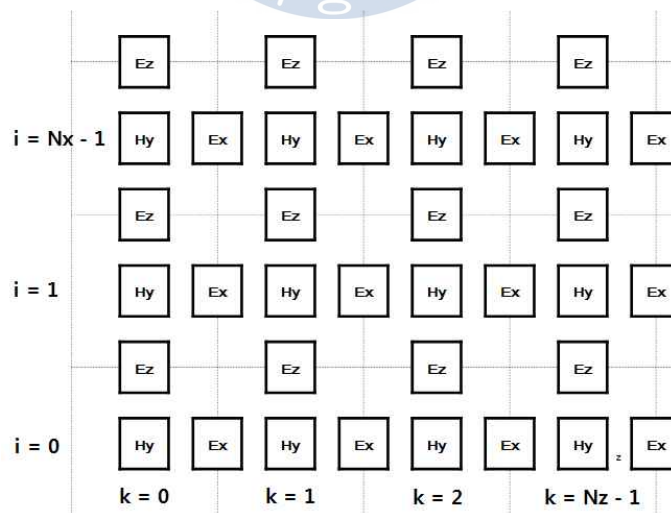


Fig. 3.5 Location of the TM fields in the computational domain.

TM mode is similar before saying TE mode. The TM fields stencil is going to explain as **Formula 12 to 12**. The E_y field locations coincide with the mesh nodes (i, k) given in 2D computational domain. Each center of grid box represent the FDTD space cell given In **Fig 3.5**. The electric fields E_x and E_z are related with cell edges. The magnetic fields (H_y) are related with integer values of the indices i and k . The electric field (x-direction E_x) is related with integer i and $(k + 0.5)$ indices. The electric field (z-direction E_z) is associated with $(i + 0.5)$ and integer k indices. The TM mode algorithm can be presented in **Formula 3.14, 3.15**.

The update equation for the z-direction and x-direction of the electric field are written by **Formula 3.14** with space-time point $\left(\left(m + \frac{1}{2}\right)\Delta_x, n\Delta_y, q\Delta_t\right)$ and **Formula 3.15** with space-time point $\left(\left(m + \frac{1}{2}\right)\Delta_x, n\Delta_y, q\Delta_t\right)$.

$$E_z^{n+1}\left[i + \frac{1}{2}, k\right] = \frac{1 - \frac{\sigma_m \Delta_t}{2\varepsilon}}{1 + \frac{\sigma_m \Delta_t}{2\varepsilon}} E_z^n\left[i + \frac{1}{2}, k\right] + \frac{1}{1 + \frac{\sigma_m \Delta_t}{2\varepsilon}} \frac{\Delta_t}{\varepsilon \Delta_x} \left(H_y^{n+\frac{1}{2}}\left[i + \frac{1}{2}, k + \frac{1}{2}\right] - H_y^{n+\frac{1}{2}}\left[i + \frac{1}{2}, k - \frac{1}{2}\right] \right)$$

$$E_x^{n+1}\left[i, k + \frac{1}{2}\right] = \frac{1 - \frac{\sigma \Delta_t}{2\varepsilon}}{1 + \frac{\sigma \Delta_t}{2\varepsilon}} E_x^n\left[i, k + \frac{1}{2}\right] - \frac{1}{1 + \frac{\sigma \Delta_t}{2\varepsilon}} \frac{\Delta_t}{\varepsilon \Delta_z} \left(H_y^{n+\frac{1}{2}}\left[i + \frac{1}{2}, k + \frac{1}{2}\right] - H_y^{n+\frac{1}{2}}\left[i - \frac{1}{2}, k + \frac{1}{2}\right] \right)$$

Formula 3.14

The electric-field update equation is obtained via the finite-difference approximation of **Formula 13** expanded about $\left(m\Delta_x, n\Delta_y, \left(q + \frac{1}{2}\right)\Delta_t\right)$

$$H_y^{n+\frac{1}{2}}\left[i + \frac{1}{2}, k + \frac{1}{2}\right] = \frac{1 - \frac{\sigma_m \Delta_t}{2\mu}}{1 + \frac{\sigma_m \Delta_t}{2\mu}} H_y^{n-\frac{1}{2}}\left[i + \frac{1}{2}, k + \frac{1}{2}\right]$$

$$- \frac{1}{1 + \frac{\sigma_m \Delta_t}{2\mu}} \left(\frac{\Delta_t}{\varepsilon \Delta_z} \left\{ E_x^n\left[i + 1, k + \frac{1}{2}\right] - E_x^n\left[i, k + \frac{1}{2}\right] \right\} - \frac{\Delta_t}{\mu \Delta_x} \left\{ E_z^n\left[i + \frac{1}{2}, k + 1\right] - E_z^n\left[i + \frac{1}{2}, k\right] \right\} \right)$$

Formula 3.15

There quantities from **Formula 3.16** simply appear in the update equations and employ the following naming convention to C language.

$$\begin{aligned}
 C_{hzh}\left(i+\frac{1}{2},k+\frac{1}{2}\right) &= \frac{1-\frac{\sigma_m\Delta_t}{2\mu}}{1+\frac{\sigma_m\Delta_t}{2\mu}} \Bigg|_{\left(i+\frac{1}{2}\right)\Delta_z,\left(i+\frac{1}{2}\right)\Delta_z} & C_{hze}\left(i+\frac{1}{2},k+\frac{1}{2}\right) &= \frac{1}{1+\frac{\sigma\Delta_t}{2\mu}} \frac{\Delta_t}{\mu\delta} \Bigg|_{\left(i+\frac{1}{2}\right)\Delta_z,\left(i+\frac{1}{2}\right)\Delta_z} \\
 C_{eze}\left(i+\frac{1}{2},k\right) &= \frac{1-\frac{\sigma_m\Delta_t}{2\epsilon}}{1+\frac{\sigma_m\Delta_t}{2\epsilon}} \Bigg|_{\left(i+\frac{1}{2}\right)\Delta_z,k\Delta_x} & C_{ezh}\left(i+\frac{1}{2},k\right) &= \frac{1}{1+\frac{\sigma\Delta_t}{2\epsilon}} \frac{\Delta_t}{\epsilon\delta} \Bigg|_{\left(i+\frac{1}{2}\right)\Delta_z,k\Delta_x} \\
 C_{exe}\left(i,k+\frac{1}{2}\right) &= \frac{1-\frac{\sigma_m\Delta_t}{2\epsilon}}{1+\frac{\sigma_m\Delta_t}{2\epsilon}} \Bigg|_{i\Delta_z,\left(k+\frac{1}{2}\right)\Delta_x} & C_{exh}\left(i,k+\frac{1}{2}\right) &= \frac{1}{1+\frac{\sigma\Delta_t}{2\epsilon}} \frac{\Delta_t}{\epsilon\delta} \Bigg|_{i\Delta_z,\left(k+\frac{1}{2}\right)\Delta_x}
 \end{aligned}$$

Formula 3.16

Following **Chapter 3.2** approach that was used in one dimension. Form as illustrated in **Fig 3.5**, an Ex node is assumed to be a half spatial step further in the z direction than the corresponding Hy node with the same indices. Similarly, an Ez node is assumed to be a half spatial step further in the x direction than the corresponding Hy node with the same indices. Finally, Translated TM mode is written by

$$\begin{aligned}
 \mathbf{Hy}(i, k) &= \text{Chyh}(i, k) * \mathbf{Hy}(i, k) + \text{Chye}(i, k) * ((\mathbf{Ez}(i, k + 1) \\
 &\quad - \mathbf{Ez}(i, k)) - (\mathbf{Ex}(i + 1, k) - \mathbf{Ex}(i, k))); \\
 \mathbf{Ez}(i, k) &= \text{Ceze}(m, n) * \mathbf{Ez}(i, k) + \text{Cezh}(i, k) * (\mathbf{Hy}(i, k) - \mathbf{Hy}(i, k - 1)); \\
 \mathbf{Ex}(i, k) &= \text{Cexe}(i, k) * \mathbf{Ex}(i, k) - \text{Cexh}(i, k) * (\mathbf{Hy}(i, k) - \mathbf{Hy}(i - 1, k));
 \end{aligned}$$

Formula 3.17

Depending on sub-wavelength scale changed sampling time. sampling is need to 10 to 20 steps wavelength to ensure numerical stability of the algorithm. This paper is used to THz wavelength scale (1THz = 300 μm). limitation of time step is decided by

$$\Delta t \leq 1 \frac{1}{c \sqrt{\frac{1}{(\Delta x)^2} + \frac{1}{(\Delta z)^2}}}$$

Formula 3.18



Chapter 4 Thin film sensing

4.1 Waveguide

4.1.1 Various Waveguide

"location movement" is always occurred around us. peoples hope to use signal or energy their home. For taking water we are using water pipe, for taking gas we are using gas pipe cable, for taking electricity we are using wire lines, for taking Internet we are using Wifi. There are many kind of connection with us in order to use energy and signal. specially, those kind of connections are called waveguide which is transfer an electromagnetic wave. Fig 4.1 show some of waveguide shapes to propagate electromagnetic effectively to move.

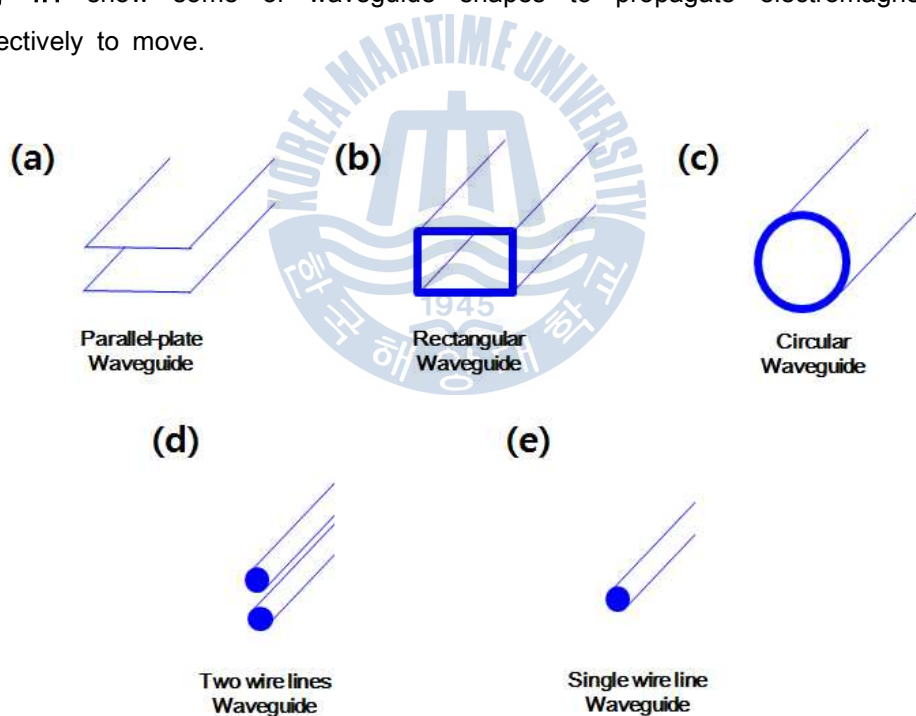


Fig. 4.1 Various Waveguide. (a) Parallel-plate Waveguide. (b) Rectangular Waveguide. (c) Circular Waveguide. (d) Two wire lines Waveguide. (e) Single wire line Waveguide.

Fig 4.1 (a) is Parallel-plate Waveguide, it has low loss and wide band THz-spectra to transfer. But when two plate distance, called air gab, is going to be far away. The gab generate a lot of mode of propagation between upper and lower plate. Structure of PPWG is difficult to bend waveguide. So, it is hard to use limited space to propagation. **Fig 4.1 (b)** is Rectangular Waveguide, it has single mode and wide-spectra propagation. But, it is specialized for CW (continue wave) source depend on single frequency. **Fig 4.1 (c)** is Circular Waveguide is good to propagate long distance by using high mode. but, Circular Waveguide has a cut off frequency at the low frequency domain. **Fig 4.1 (d)** is Two wire lines Waveguide, is has similar shape with propagation filed shape. So, two wire has high coupling efficiency and it is strong for bending-loss compare with single wire. Two wire has TEM propagation mode. that means is no cut off frequency through two wire. **Fig 4.1 (e)** is single wire, it have low loss and no group velocity dispersion. But, coupling efficiency is very low from dipole antenna as well as bending-loss.

There are many different shape Waveguide, which are Parallel-plate Waveguide, Rectangular Waveguide, Circular Waveguide, Two wire lines Waveguide and Single wire line, include pros and cons. This paper chose parrel-plate waveguide, which is the most simple structure consider about cost and analysis and low loss and broad band THz spectra. We have already many technique by using PPWG. Next page speak about PPWG technique when we do experiment.

4.1.2 PPWG Techniques

Schematic diagram of the thin film from **Fig 4.2 (a)**. For improving THz pulse coupling efficient to the plate-separation air gap, we use a tapered parallel plate waveguide (TPPWG) without a cylindrical silicon lens. coupling efficient is around 2 time higher than used cylindrical lens. A single slit sheet is located in the middle of the TPPWG air gap to divide the two channels.

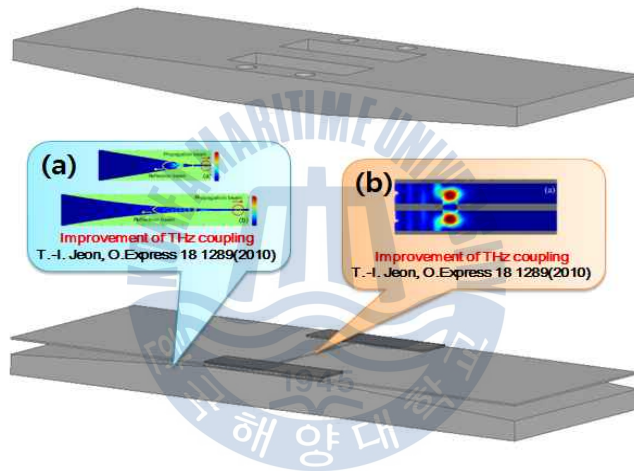


Fig. 4.2 Schematic waveguide and technique. **(a)** Improvement of THz coupling using a tapered parallel-plate waveguide [9], **(b)** Terahertz band gap properties by using metal slits in tapered parallel-plate Waveguide. [10]

A single slit divide two pulse and make time delay between two pulse. It cause making high resonance. Slit and air gab affected resonance frequency and Q-factor. resonance can apply to many kind of way. For example thin film spectroscopy an THz pulse notch or band pass filters.

4.2 What is thin film

What exactly constitutes a Thin film? This paper write down about thin film is sample that results in overlapping between the main transmitted pulse and the partial internal reflections. [11-17]

4.3 Method of thin film sensing

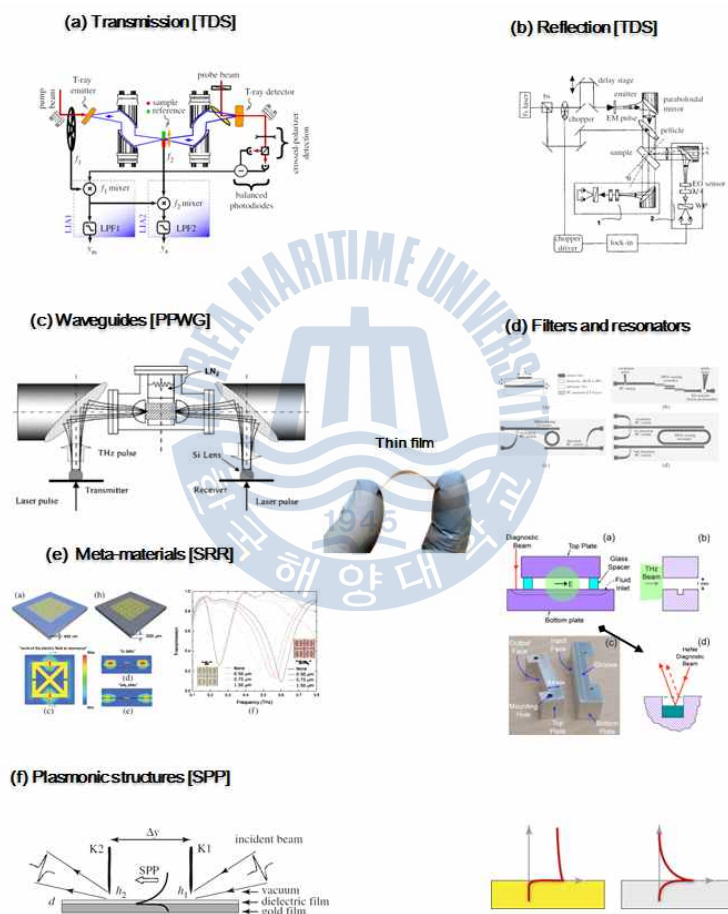


Fig. 4.3 THz thin-film Sensing. (a) Transmission-mode with THz-TDS, (b) Reflection-mode with THz-TDS, (c) Waveguide, (d) Filters and resonators, (e) Matamaterials, (f) Plasmonic structures.

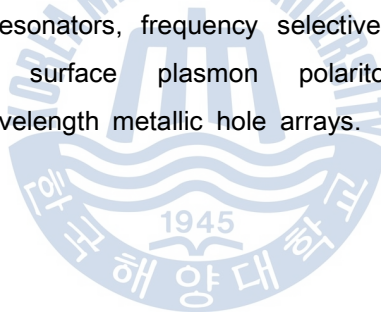
There are the six most reported methods, Transmission-mode with THz-TDS, reflection-mode with THz-TDS, waveguide, filters and resonators, metamaterials, plasmonic structures, of THz thin film sensing.

Fig 4.3 (a) to (c) provide quantitative complex optical properties, or at least spectral absorption lines spanning a wide bandwidth.

Fig 4.3 (a) is transmission, THz time domain interferometry, THz differential time domain spectroscopy. **Fig 4.3 (b)** is reflection, thin film interference THz goniometry, THz ellipsometry. **Fig 4.3 (c)** is waveguide, parallel plate waveguides, micro-strip transmission lines.

Fig 4.3 (d) to (f) have a detection nature meaning they usually indicate the presence or change of a sample without necessarily identifying or characterizing it.

Fig 4.3 (d) is filters and resonators, filter-loaded transmission lines, cavity resonators in waveguide. **Fig 4.3 (e)** is metamaterials, split-ring resonators, asymmetric split ring resonators, frequency selective surface. **Fig 4.3 (f)** is plasmonic structures, surface plasmon polaritons on metals and semiconductors, sub-wavelength metallic hole arrays.



4.4 PPWG : Parallel-plate Waveguide Sensing

4.4.1 Simulation condition

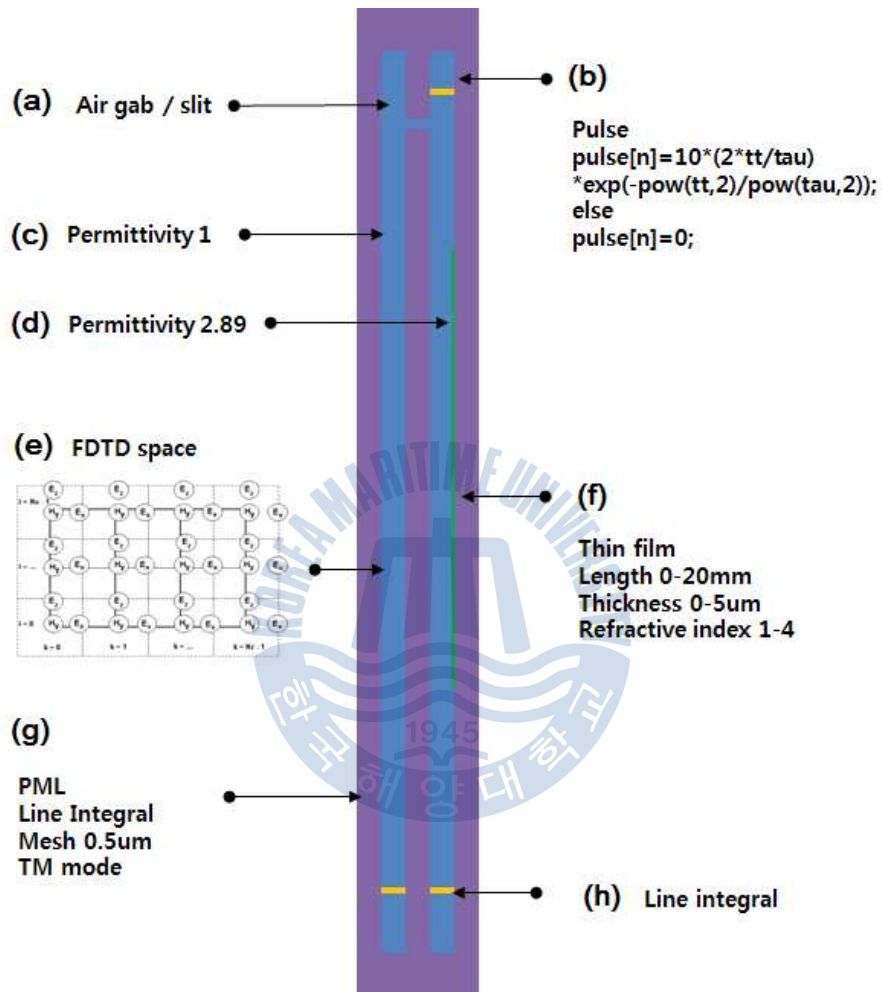


Fig. 4.4 Schematic of 2D FDTD simulation space. (a) air gab is 100 μm and silt width is 60 μm , (b) gaussian pulse equation, (c) free space permittivity, (d) dielectric permittivity, (e) Magnetic and electric space in FDTD, (f) thin layer range of length, thickness, refractive index, (g) boundary condition and mesh size, (h) acquiring data line.

Fig 4.4 is Schematic of 2D FDTD simulation space. Thin film length, thickness and refractive index are 0 to 20 mm, 0 to 5 μm and 1 to 5. Each THz pulse wave along z-direction are 100 μm thickness, slit width is 60 μm . Considering thin film length include slit and boundary condition should be decide space size. So, z-direction FDTD space is 22 mm. Space size and thin film thickness decide calculation time by using FDTD simulation. If consider about maximum 20 mm of thin film and limited thickness of thin film. FDTD simulation space is 22mm include slit and boundary conditions and mesh size is to be 0.5 μm to calculate 0.5 μm thickness of thin film.

z-direction number of cell is 44000, 22 mm divided 0.5 μm size, and x-direction number of cell is 640, 320 μm divided 0.5 μm . One step of time space need to do 28,160,000 times of calculation. then, 0.5 μm of mesh size need to 160000 times mesh size to pass in PPWG. Total time domain scan range is 133 ps. 2D FDTD simulation need to 4.5056×10^{12} times calculation. It is very huge calculation to do predict resonance shift by use FDTD method. General computer have limited memory and CPU to calculate big array. To over come limitation of computer, we used supercomputer at KISTI supercomputing service center where is located at the DeaJeon as well as C language is programed using 4 CPU to reduce calculation time. So, each FDTD simulation calculation spend 16 to 20 hours depend on condition of simulation. Even though reducing mesh size can get detail information of thin film, but we decided mesh size at 0.5 μm .

Simulation pulse is generated by using gaussian equation. Pulse spectra band width is adjusted like experiment result of band width, 0 to 3 THz, by controlling value of tau in **Fig 4.4** pulse equation. After calculating FDTD simulation, result is acquired by using line integral method. FFT fourier transform is done with 10 time zero padding to make narrow frequency step.

4.4.2 Simulation : Thin film sensing

1) FDTD Simulation : Thin film Dependent-length

Thin film Dependent-length ($n = 1.7$, thickness $1.0 \mu\text{m}$)

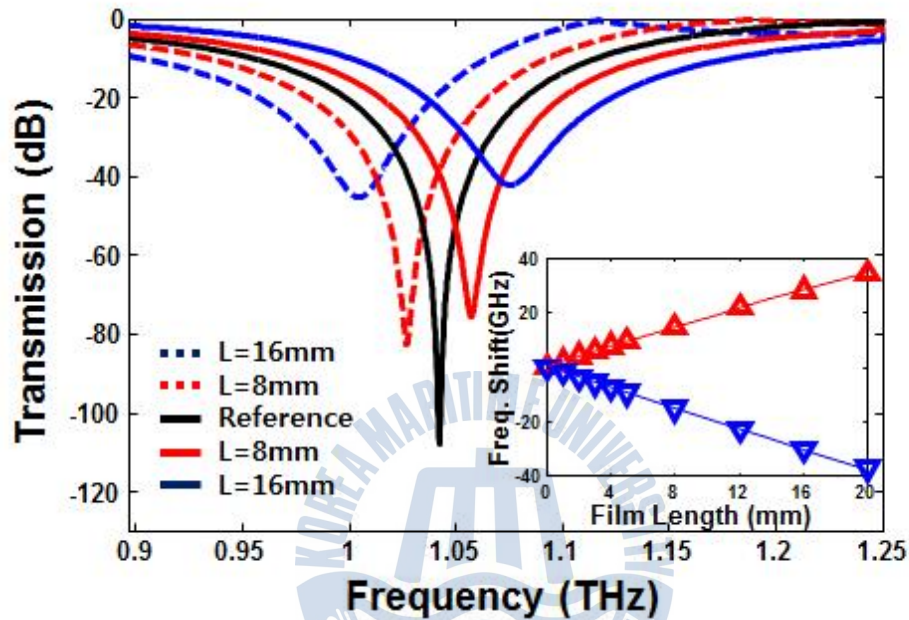


Fig. 4.5 The transmission spectra of the length-dependent resonances, which are 0 to 20 mm in length with a fixed thickness of $1.00 \mu\text{m}$ and a refractive index of 1.7. Solid lines indicate that the upper channel is open and the lower channel is close. dot lines indicate that the lower channel is open and the upper channel is close. **Insert** : frequency shifts for different film lengths. thin film respectively, for the open upper channel (red triangles) and for the open lower channel (inverse blue triangles).

FDTD simulations were performed to verify waveguide sensing possibility. Various conditions for the thin film on the PPWG surface were simulated and discussed in **chapter 4.4.1 to 4.4.5**. The dimensions of the PPWG and slit

were the same as those described, waveguide structure; however, the refractive index, thickness, and length of the thin film were set 1.7, 1.00 μm , and 1 mm, respectively, consider about the limited scale size of the calculations.

Fig. 4.5 Solid lines indicate that the upper channel is open and the lower channel is close. The dashed lines indicate the reverse case. The transmission spectra of the length-dependent resonances, which are 0 to 20 mm in length with a fixed thickness of 1.00 μm and a refractive index of 1.7, are shown in **Fig 4.5**

Table 4.1 Simulation : Resonance point of length-dependent Thin Film

		Unit (mm)								
Input	ref	1	2	3	4	5	8	12	16	20
upper	1.0419	1.0439	1.0459	1.0478	1.0496	1.0513	1.0568	1.0638	1.0703	1.0764
lower	1.0419	1.0403	1.0384	1.0365	1.0346	1.0327	1.0268	1.0193	1.0119	1.0048

Refractive index 1.7, Thickness 1.0 μm

Table 4.1 Show thin film length-dependent shifting resonance frequency, which linearly changes with increasing frequency. FTS, Frequency turning sensitivity, is calculated **1.73** and **-1.86 GHz/mm** for only open upper channel and only open lower channels, respectively.

Thin film Dependent-length ($n= 1.7$, thickness $1.5 \mu\text{m}$)

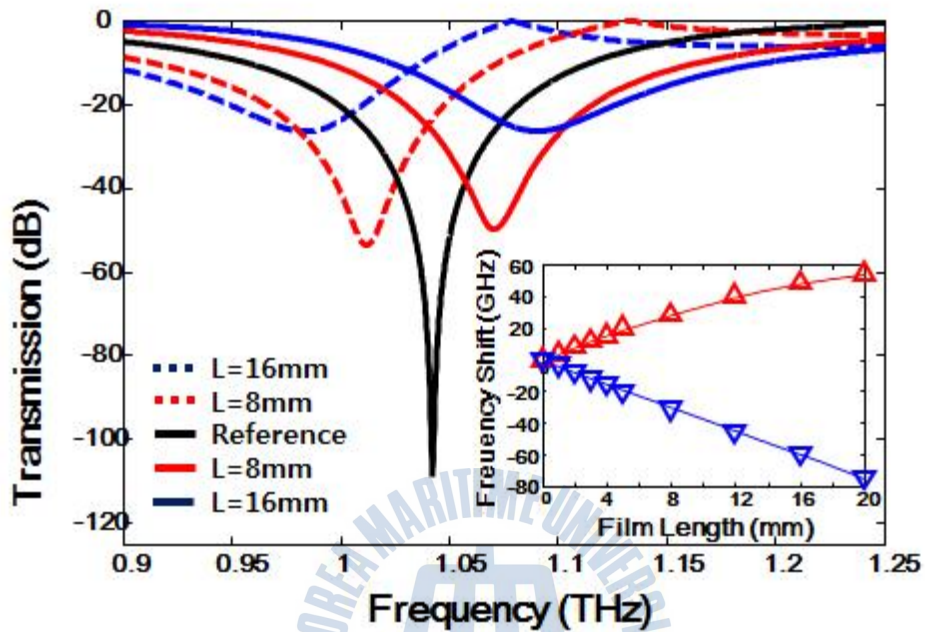


Fig. 4.6 The transmission spectra of the length-dependent resonances, which are 0 to 20 mm in length with a fixed thickness of $1.50 \mu\text{m}$ and a refractive index of 1.7. Solid lines indicate that the upper channel is open and the lower channel is close. dot lines indicate that the lower channel is open and the upper channel is close. **Insert** : frequency shifts for different film lengths. thin film respectively, for the open upper channel (red triangles) and for the open lower channel (inverse blue triangles).

The transmission spectra of the length-dependent resonances, which are 0 to 20 mm in length with a fixed thickness of $1.5 \mu\text{m}$ and a refractive index of 1.7, are shown in **Fig 4.6** and **Table 4.2**. The table show thin film length-dependent frequency shifts, which linearly changes with increasing

resonance frequency. The calculated FTS is **2.71 and -2.74 GHz/mm** for the open upper and lower channels, respectively.

Table 4.2 Simulation : Resonance point of length-dependent Thin Film

Input	ref	Unit (mm)								
		1	2	3	4	5	8	12	16	20
Upper	1.0419	1.045	1.05	1.054	1.057	1.062	1.07	1.082	1.09	1.096
Lower	1.0419	1.039	1.034	1.03	1.027	1.022	1.011	0.996	0.982	0.967

Refractive index 1.7, Thickness 1.5 μm

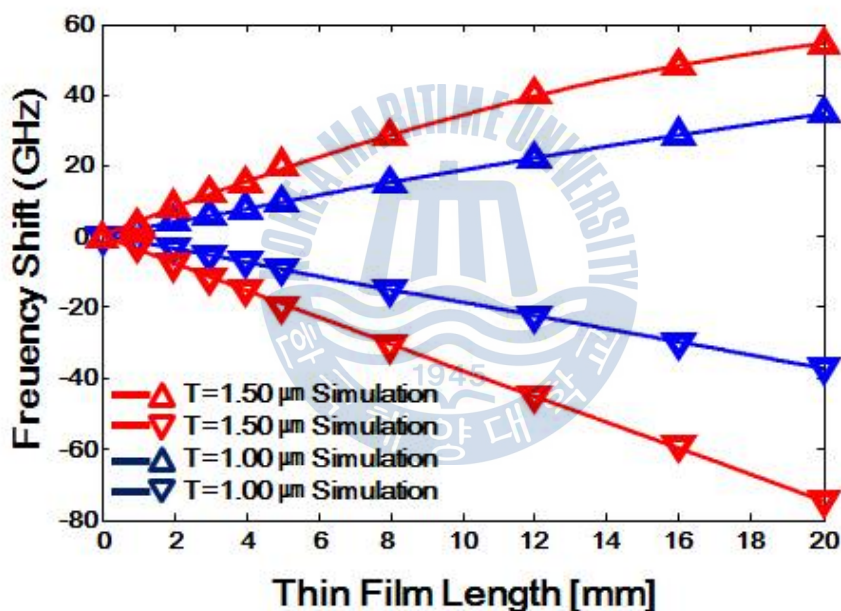


Fig. 4.7 Compared thickness 1.0 μm and 1.5 μm thin film depend on frequency shifts for different thin film lengths. thin film respectively, for the open upper channel (triangles) and for the open lower channel (inverse triangles). thickness 1.50 μm length-dependent frequency shift fitting line (red line), thickness 1.00 μm length-dependent frequency shift fitting line (blue line).

Each length-dependent FDTD simulation, thickness of thin film are 1.0 μm and 1.5 μm , show us trend of the resonance shift. thin film resonance shift, which is 1.5 μm thickness is bigger than 1.0 μm from **Fig 4.7**. the factor of shifting resonance point are caused not only thin film length-dependent but also thickness-dependent. We are going to figure out thickness-dependent trend by using FDTD simulation



2) FDTD Simulation : Thin film Dependent-thickness

Thin film Dependent-thickness ($n = 1.7$, length 1.0 mm)

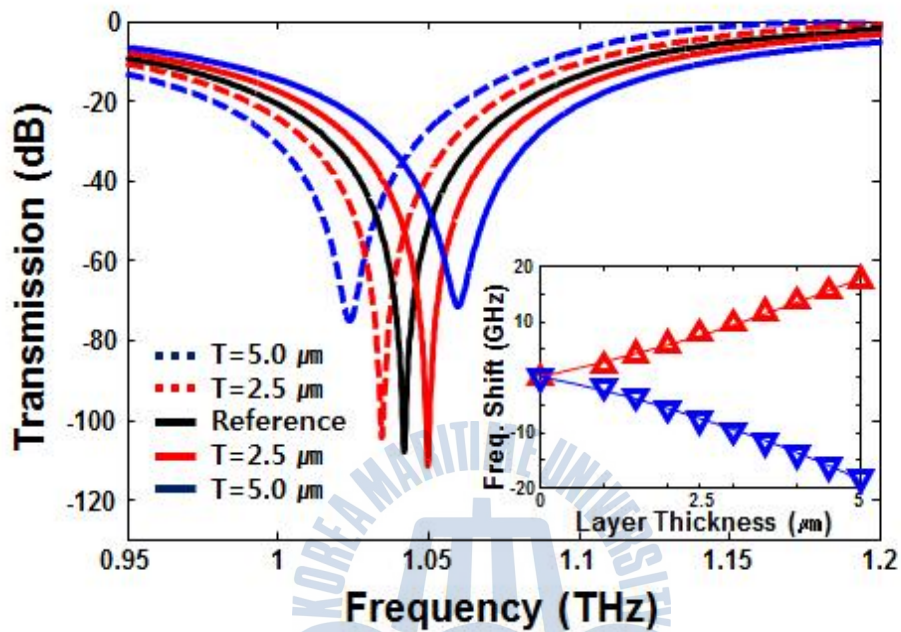


Fig. 4.8 The transmission spectra of the thickness-dependent resonances, which are 0 to 20 mm in length with a fixed thickness of 1.50 μm and a refractive index of 1.7. Solid lines indicate that the upper channel is open and the lower channel is close. dot lines indicate that the lower channel is open and the upper channel is close. **Insert** : frequency shifts for different film lengths. thin film respectively, for the open upper channel (red triangles) and for the open lower channel (inverse blue triangles).

Pre-simulation predict thin film dependent-length resonance shift. Thin film has two option 1.0 μm and 1.5 μm . Resonance shift is caused not only length of thin film but also thickness of thin film. Thickness difference

between two thin film range of resonance shift indicate influence of thickness. To know how much relate between thin film thickness and resonance shift. FDTD simulation is done with fixing reference like that refractive index, thickness and length of the thin film were set (reference condition) 1.7, 1.00 μm , and 1 mm.

Table 4.3 Simulation : Resonance point of thickness-dependent thin film

		Unit (μm)								
Input	ref	1	2	3	4	5	8	12	16	20
upper	1.0419	1.0439	1.0459	1.0478	1.0498	1.0517	1.0537	1.0557	1.0575	1.0595
lower	1.0419	1.0403	1.0384	1.0363	1.0343	1.0322	1.0302	1	1.0258	1.0236

Refractive index 1.7, Length 1 mm

To simulate 0.5 μm thickness need to make mesh size at least 0.5 μm . Even though, it is nice to reduce mesh size. But we should select 0.5 μm because of limitation of FDTD calculation. Why minimized thickness is 0.5 μm .

The transmission spectra of the thickness-dependent, 0 to 5 μm thickness with a fixed length of 1 mm and a refractive index of 1.7, are shown in **Fig 4.8**. The table show thin film dependent-thickness resonance shifts. Table 4.3 show resonance shifts that is linearly changed resonance frequency. FTS, frequency turning sensitivity, is calculated **0.88 and -0.912 GHz/mm**.

3) FDTD Simulation : Thin film Dependent-refractive index

Thin film Dependent-refractive index ($n = 1.7$, length 1.0 mm)

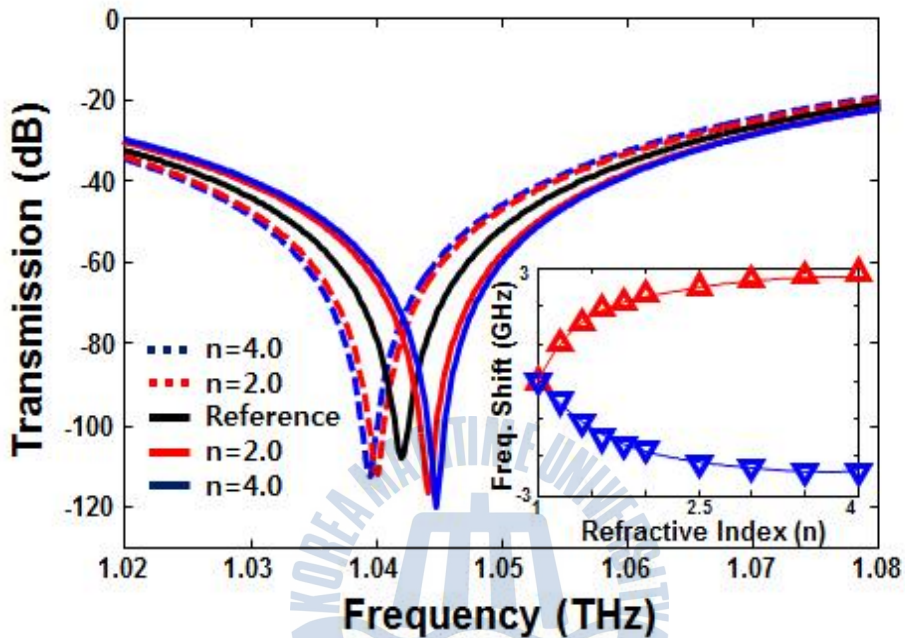


Fig. 4.9 The transmission spectra of the refractive index-dependent resonances shift, which are 1 to 4 refractive index with a fixed thickness of $1.50 \mu\text{m}$ and a length of 1mm. Solid lines indicate that the upper channel is open and the lower channel is close. Dot lines indicate that the lower channel is open and the upper channel is close. **Insert** : frequency shifts for different film refractive index. Thin film respectively, for the open upper channel (red triangles) and for the open lower channel (inverse blue triangles).

Thin film length and thickness have relation with resonance shift. Other important point is expected to be refractive index. In this simulation try to figure out refractive index with resonance shift.

Basic thin film condition of FDTD simulation, refractive index, thickness and length of the thin film were set (reference condition) 1.7, 1.00 μm , and 1 mm, respectively, because of the limited scale size of the calculations. **Figure 4.9** shows the transmission spectra of refractive index-dependent resonances. The refractive index changed from 1 to 4.

Table 4.4 Simulation : Resonance point of refractive index-dependent Thin Film

Input	ref	Unit (μm)								
		1	2	3	4	5	8	12	16	20
Upper	1.0419	1.0429	1.0435	1.0438	1.044	1.0442	1.0444	1.0446	1.0447	1.0448
Lower	1.0419	1.0414	1.0408	1.0404	1.0402	1.0401	1.0397	1.0396	1.0395	1.0395

Refractive index 1.7, Thickness 1.0 μm

Fitting lines, resonance shift, the insets in **Fig 4.7, 4.8** and the inset in **Fig 4.9**, shows that the frequency shift is proportion by length and thickness. But refractive index-dependent line, resonance shift, is going to saturation from 2.5 THz roughly. The refractive index in **Fig 4.9** changes from 1 to 4 with a fixed 1 mm thin film length and a 1.00 μm thickness.

2D FDTD simulation predict trend of thin film sensitivity with PPWG. Resonance shift is done depend on thin film length, thickness and refractive index. Dependent length and thickness has linear shift. But refractive index is going to saturation when refractive index bigger than bigger.

4.4.3 Experiment : Set up & Thin film

1) Experiment : Set up

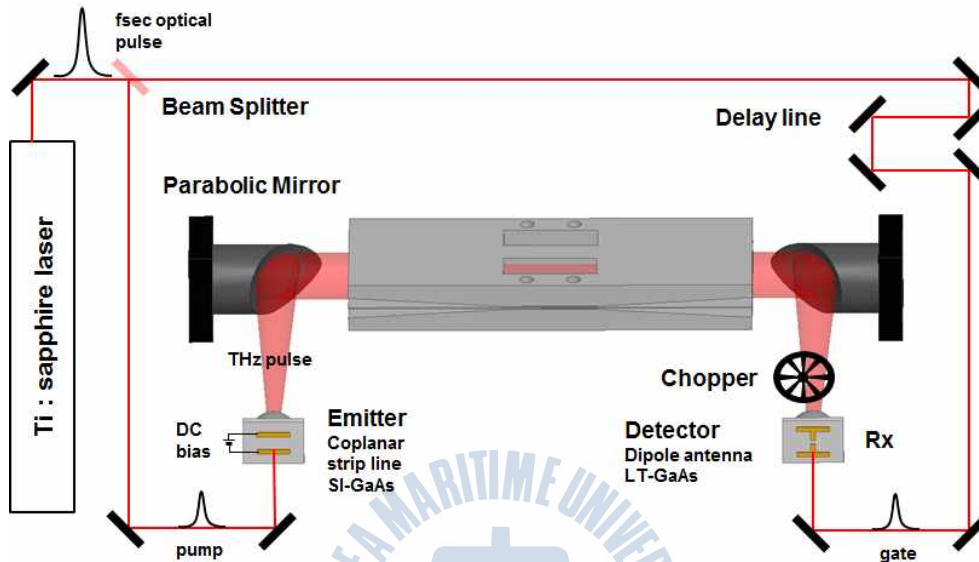


Fig. 4.10 Schematic diagram of THz time domain system with PPWG between two parabolic mirrors.

Terahertz time-domain spectroscopy is the study of material properties using time-resolved sub-picosecond THz pulses with frequency content between 0.1 and 5 THz. Typically, biased photo-conductive semiconductor antenna with an optical pulse, resulting in THz pulse. This THz pulse is collimated by a high-resistivity Si lens and a parabolic mirror, then coupled with Waveguide and make mode and propagate in the waveguide, then under investigation, and finally refocused onto a gated semiconductor photo-conductive antenna, which acts as a detector.

Measurement with a frequency resolution of 0.6 GHz and signal-to-noise (S/N) ratio of 16613 can be achieved without waveguide. The entire system is located in an airtight enclosure to mitigate the effects of water vapor on the THz pulse. A high-performance opto-electronic source chip, used to

generate pulses of freely propagating. The simple coplanar transmission line structure of the chip consists of two 10 μm wide metal lines separated by 80 μm , fabricated on high resistivity Si-GaAs. Irradiating the metal-semiconductor interface (edge) of the positively biased line with focused optical pulses produces synchronous bursts of THz radiation. This occurs because each optical pulse creates a spot of photo carriers in a region of extremely high electric field. The consequent acceleration of the carriers generates the burst of radiation. This experiment used Maitai Laser, titanium sapphire laser with 780 nm, 60 fs excitation pulses, optical pulse attenuate average power of 15 mW at the 5 μm diameter excitation spot. The major fraction of the laser-generated burst of THz pulse is emitted into the LT-GaAs substrate in a cone normal to the interface and is then collected and collimated by a crystalline high-resistivity silicon lens attached to the back side of the chip.

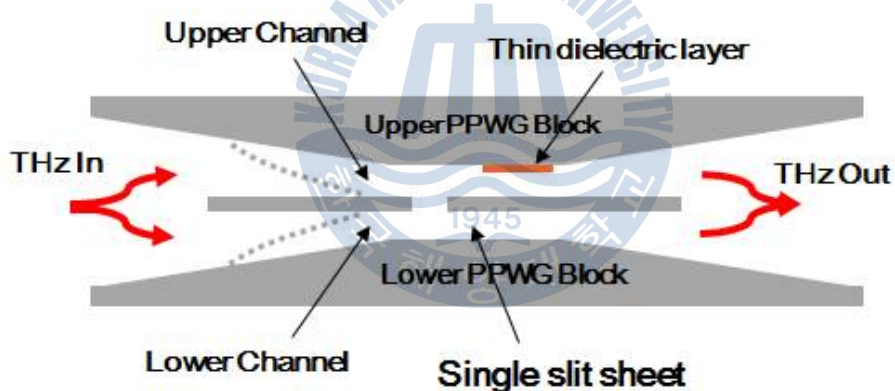


Fig 4.11 The waveguide structure. A single slit sheet is located in the middle of the PPWG air gap to divide the two channels. The front part of the sheet can be bent in an upper or lower direction (indicated by the dashed lines) to open only one of the channels. A thin dielectric layer (SU-8) is on the upper PPWG block surface.

Waveguide is located between parabolic mirrors which is made by aluminium. whole width is 63 mm and height length is 172 mm.

Upper side plate has holes. this holes procure bolt to hold metal sheet and spacer. and, strongly fixed slit and spacer make stability to keep air gab between two plate. Single slit structure is completed with arc discharged PPWG. Arc discharge provide uniform surface of PPWG and improve THz pulse propagation in PPWG. To prevent to floating, PPWG have heavy weight. Fig 4.12 combined upper plate with lower plate with single slit.

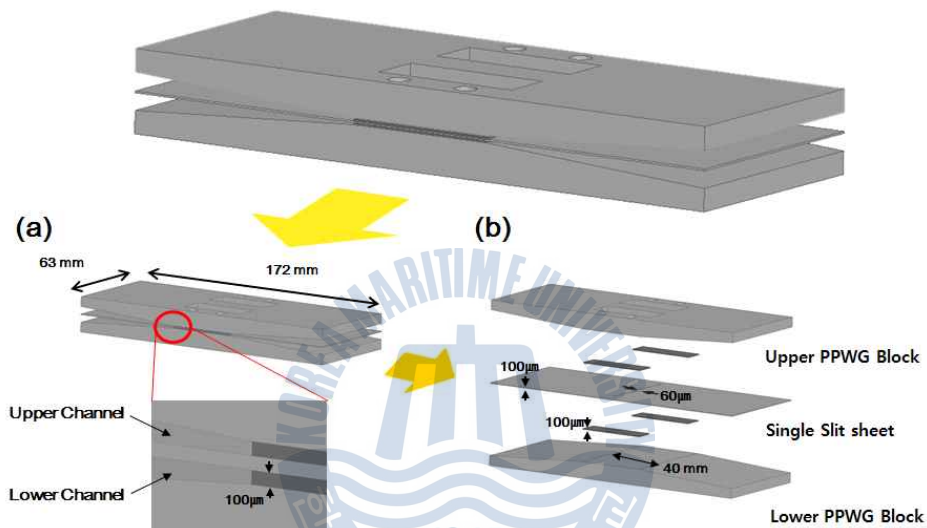


Fig 4.12 The waveguide structure. (a) Total, Waveguide width and hight length are 63 mm and 172 mm. (b) A single slit sheet is located in the middle of the PPWG and spacer to divide the two channels. aluminum spacer make 100 μm air gab each of channels. metal sheet has single slit which is 60 μm width.

Aluminum sheet with single slit is extended until edge of PPWG. When extended sheet attached to upper plate. Only open lower channel. When extended sheet attached to lower plate. Only open upper channel. To hold up metal sheet, triangle sponge is installed between two plate.

2) Experiment : making Thin film

This experiment need to make various thin film in order to know sensitivity of PPWG. A photoresist is good material for making various thin film. A photoresist is a light-sensitive material used in several industrial processes, such as photo lithography and photoengraving to form a patterned coating on a surface. At semiconductor, PR is used to make thin layer by using spin coating method.

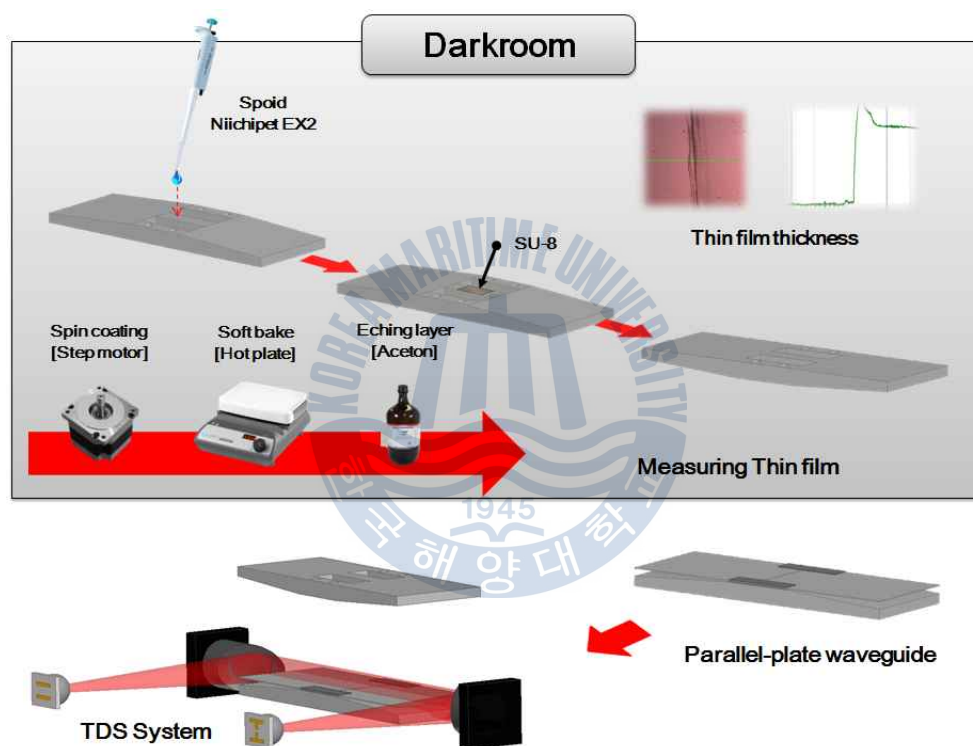


Fig. 4.13 Process, product thickness-dependent thin film samples. **Step 1** : Spin coating, drop the PR (photo resistor) on the PPWG controlled speed by using step motor. **Step 2** : Soft bake at 150 degrees, 20 Minute to 25 Minute to make hard samples. Be completed thin film on the PPWG easily can measure combined with lower sid of plate like upper picture.

Spin coating is called PR coating. dispensed liquid spreaded on surface like thin film by using high speed of rotation. Solvent of PR is removed after baking at uniformed temperature. There are different method. For example PVD, CVD. PPWG is big to be rotated and consist of metal. When metal is in chamber is caused pollution of chamber. But, we can easily build up spin coating system **Fig 4.13**.

We need to consider about relation between PPWG weight and motor condition, which are torque and RPM. Step motor and wave guide hold up by using screw to prevent to vibration of PPWG. Photoresist thickness is determined depend on time, viscosity of PR and speed of motor. We try to make thin film depend on speed of motor and time. **Table 4.5** show us speed and time dependent thickness of thin film in our spin coating system.

Table 4.5 Thin film thickness depend on speed of motor

	Unit (μm)				
Thickness	0	0.7	1.4	2.4	2.8
RPM	1.0419	1.0429	1.0435	1.0438	1.044
Time	60	60	60	60	60
Error (μm)	1.0419	1.0414	1.0408	1.0404	1.0402
Refractive index 1.7, Thickness 1.0 μm					

Spreaded PR need to soft bake that is vaporized PR to make hard. After spin coating, thin film and waveguide put on the hot plate. soft bake time is a half hour around 200 temperature. We did experiment without light until process of soft bake. photoresist react cause of light.

Completed thin film directly measured thickness by using AFM (Atomic Force Microscopy). We measured thickness selected 8 points. Thickness is calculated average without maximum and minimum thickness. **Fig 4.13** in set picture is boundary of the thin film. These error can understand under experiment error. Prediction and experiment result show us similar result.

4.4.4 Experiment : Thin film sensing

1) Experiment : Thin film Dependent-Length

Thin film Dependent-length ($n = 1.7$, thickness $1.0 \mu\text{m}$ and $1.42 \mu\text{m}$)

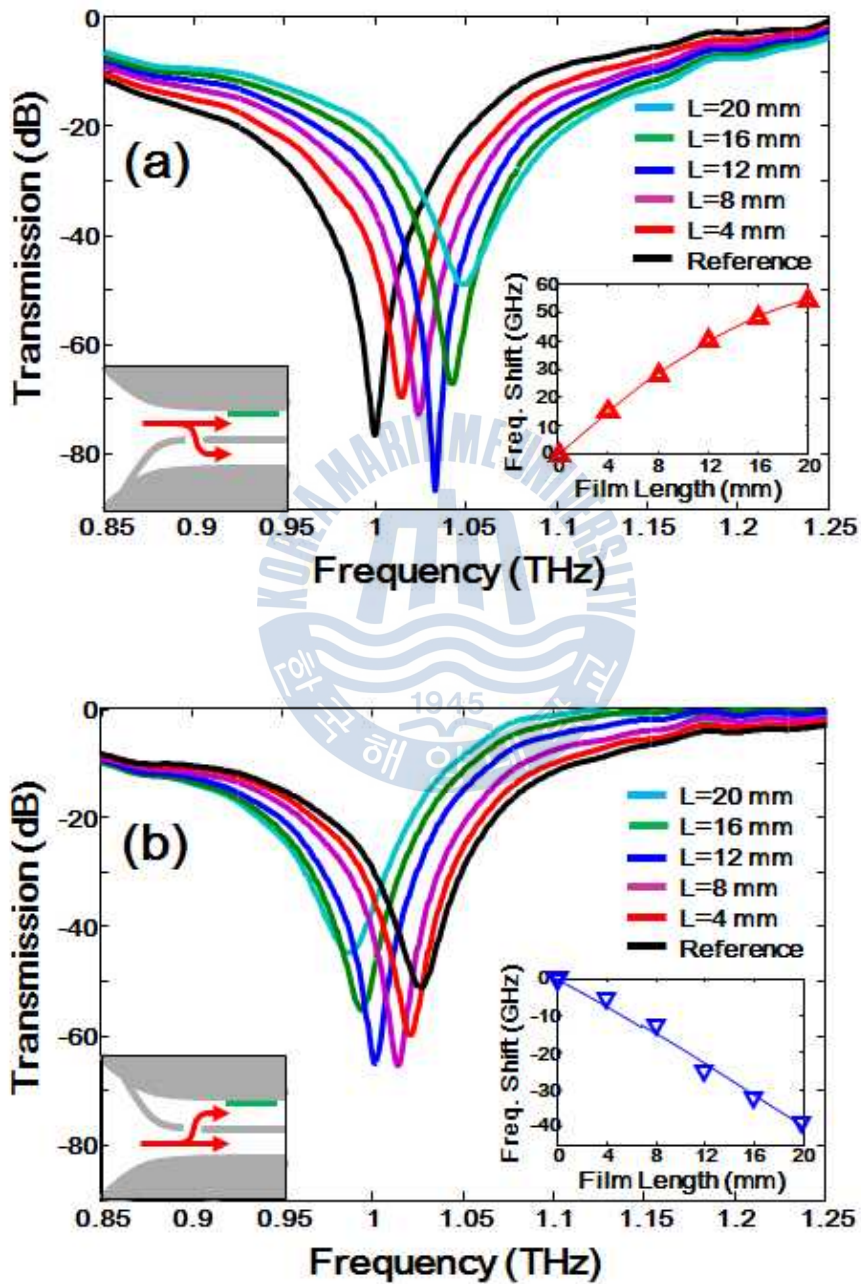


Fig 4.14 Measured transmission spectra for different film lengths. Lower right insets show the normalized reference spectrum (no coated layer). Lower left insets show the slit sheet bent in a lower or upper direction. **(a)** The input THz beam travels to the upper channel only. **(b)** The input THz beam travels to the lower channel only.

Thin film dependent-length experiment did divide two step, only open upper channel and only open lower channel, to minimize experiment errors during changing system between reference to signal. This two experiment have different thickness of thin film. Only open upper channel has $1.33 \pm 0.18 \mu\text{m}$ thickness of thin film. Only open lower channel has $1.04 \pm 0.08 \mu\text{m}$ thickness of thin film. thin film length is same. Range in **Fig 4.14 (a) and (b)** insert figures, which is shift resonance, is wider than only open lower channel which is $1.04 \pm 0.08 \mu\text{m}$ thickness. Two of FTS, which is frequency turning sensitivity, is given as $\Delta t/\Delta L$, where Δt and ΔL are the time shift and thin film length variations. **FTS is calculated 2.41 GHz/mm and -1.95 GHz/mm.**

Table 4.6 Experiment : Resonance point of length-dependent Thin Film

Input	Unit (μm)					
	ref	4	8	12	16	20
upper	0.9999	1.014	1.024	1.033	1.042	1.048
lower	1.0263	1.0208	1.0137	1.001	0.9939	0.9873

Refractive index 1.7, Thickness $1.33 \pm 0.18 \mu\text{m}$ or $1.04 \pm 0.08 \mu\text{m}$

During experiment did with inchange condition depend on thin film measurement. Thin film is removed from 20 mm to reference. THz input is adjusted to maximize signal. Extended sheet is holding by using triangle sponge to keep coupling efficient. TTS, which is Time turning sensitivity, is given as $\Delta f/\Delta L$, where Δf and ΔL are the frequency shift and thin film length variations. **TTS is 11.9 fs/mm and -2.5 fs/mm.**

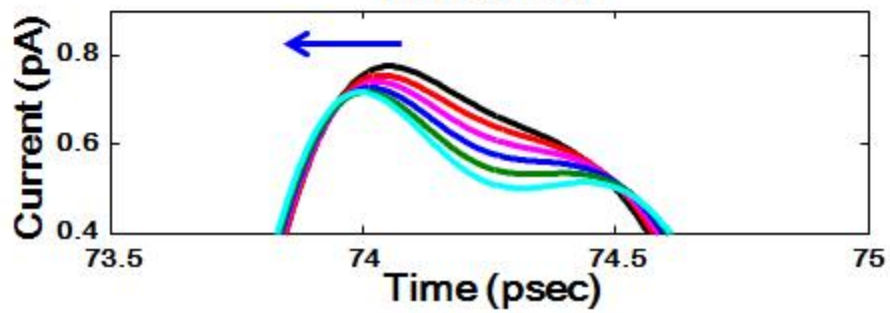
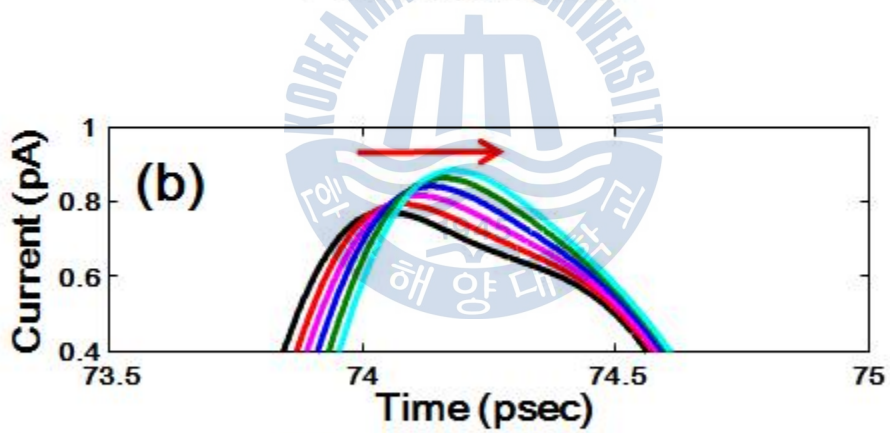
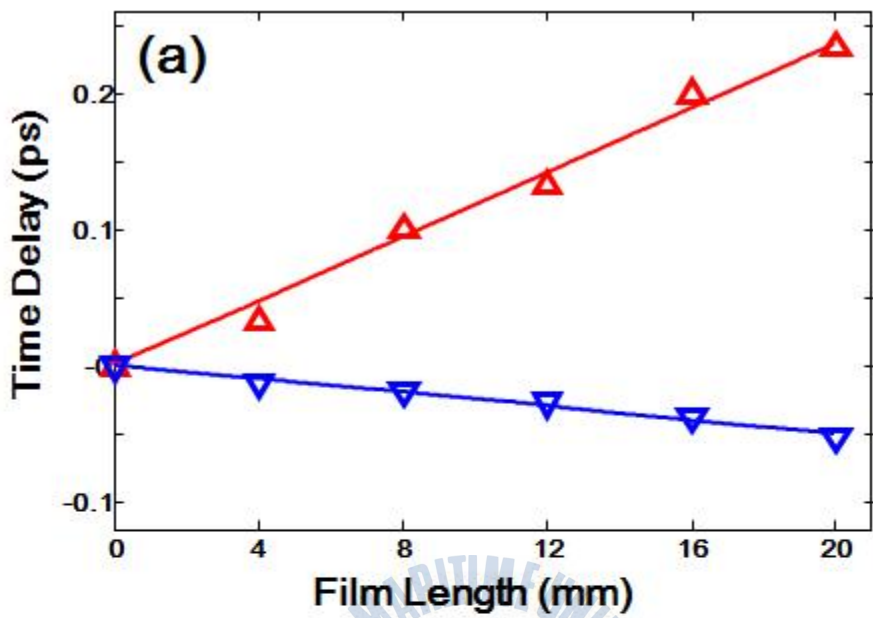


Fig. 4.15 Measured time delay. The red and blue fitting lines indicate the upper and lower channel open only respectively. **(a)** time delay depend on different film length. **(b)** time delay of THz pulse.

As show **Fig 4.15 (a), (b)** two peak of pulses shift to positive and negative. Only open upper channel is more shift than only open lower channel. The reason is when main pulse meet with thin film affected time shift better than leak out slit pulse. Even though pulse divided two pulse but, pulse amplitude is only open upper channel bigger than other one. When pulse combined upper and lower channel again. Main pulse, which directly propagate through PPWG, has influence to time domain pulse shape strongly.

The other way only open lower channel, leak out slit pulse has interaction with thin film. It is not enough to compare with main pulse interaction. So, time shift range of only open lower channel is shorter than other side of channel.

Fig. 4.15 (a) show us two case of TTS. The case of only open upper channel, if thin film length is longer than longer. Cause of slit time delay is shorter than thin film delay. Resonance shift is going to be reverse. it mean shift direction is changed. Input pulse should be upper channel which has thin film inside of channel. Time turning sensitivity should be good.

2) Experiment : Thin film Dependent-thickness

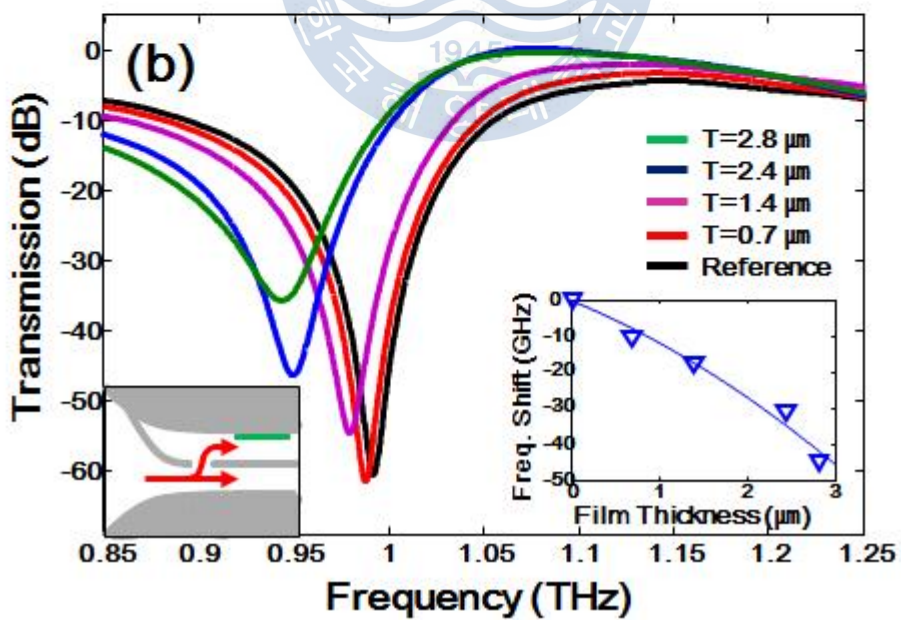
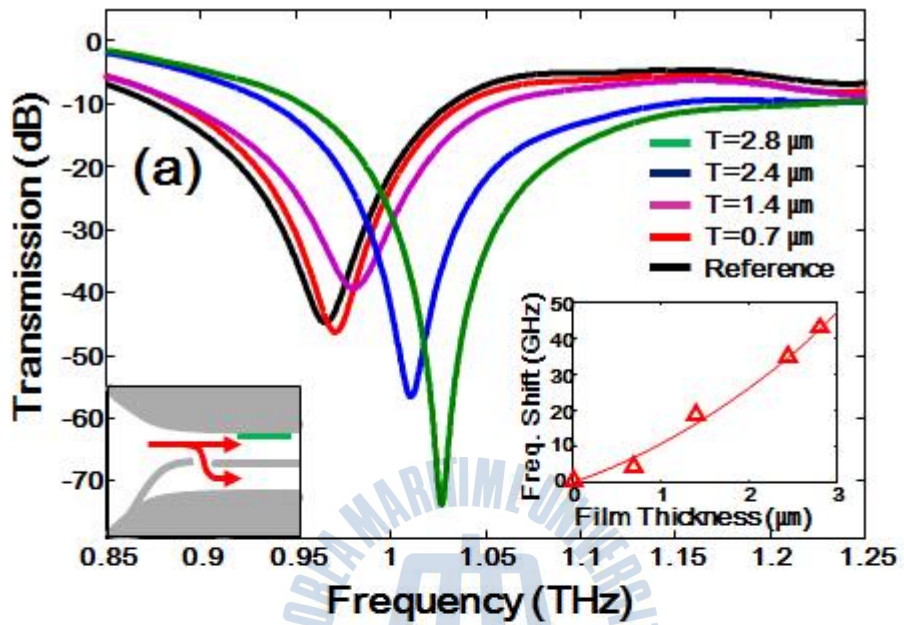


Fig. 4.16 Measured transmission spectra for different film thickness. Lower right insets show the resonance shift. Lower left insets show the slit sheet bent in a lower or upper direction. (a) The input THz pulse travels to the upper channel only. (b) The input THz pulse travels to the lower channel only.

Dependent-thickness experiment have possibility making experiment error during experiment compare with dependent-length experiment. Several times, thin film is produced in order to make different thickness of film. These process are biggest error point in dependent-thickness experiment. Most of these errors come from when setup is changed.

To minimize experiment errors, wave guide system is optimization. Thin films are produced at the earliest practicable time. Films are directly measured it is thickness. Next step is measuring only open upper channel with thin film on PPWG. Than, changing metal sheet position to only open lower channel. Finally, to do experiment process of reverse. These step are considered step of work to prevent to changes during experiment. Each step of experiment is done two times.

Table 4.7 Experiment : Resonance point of thickness-dependent Thin Film

		Unit (μm)			
Input	ref	0.693	1.398	2.446	2.815
upper	0.9663	0.9705	0.9921	1.008	1.024
lower	0.9975	0.9873	0.9801	0.9663	0.9525

Refractive index 1.7, Thickness 1.0 μm

Other errors are thin film length and thickness. Error of thickness is less than 0.1 μm , error of the length is less than 1 μm . Those factor is not affected our result. Because, our prediction and experiment result show us similar result.

4.4.5 Experiment and Simulation

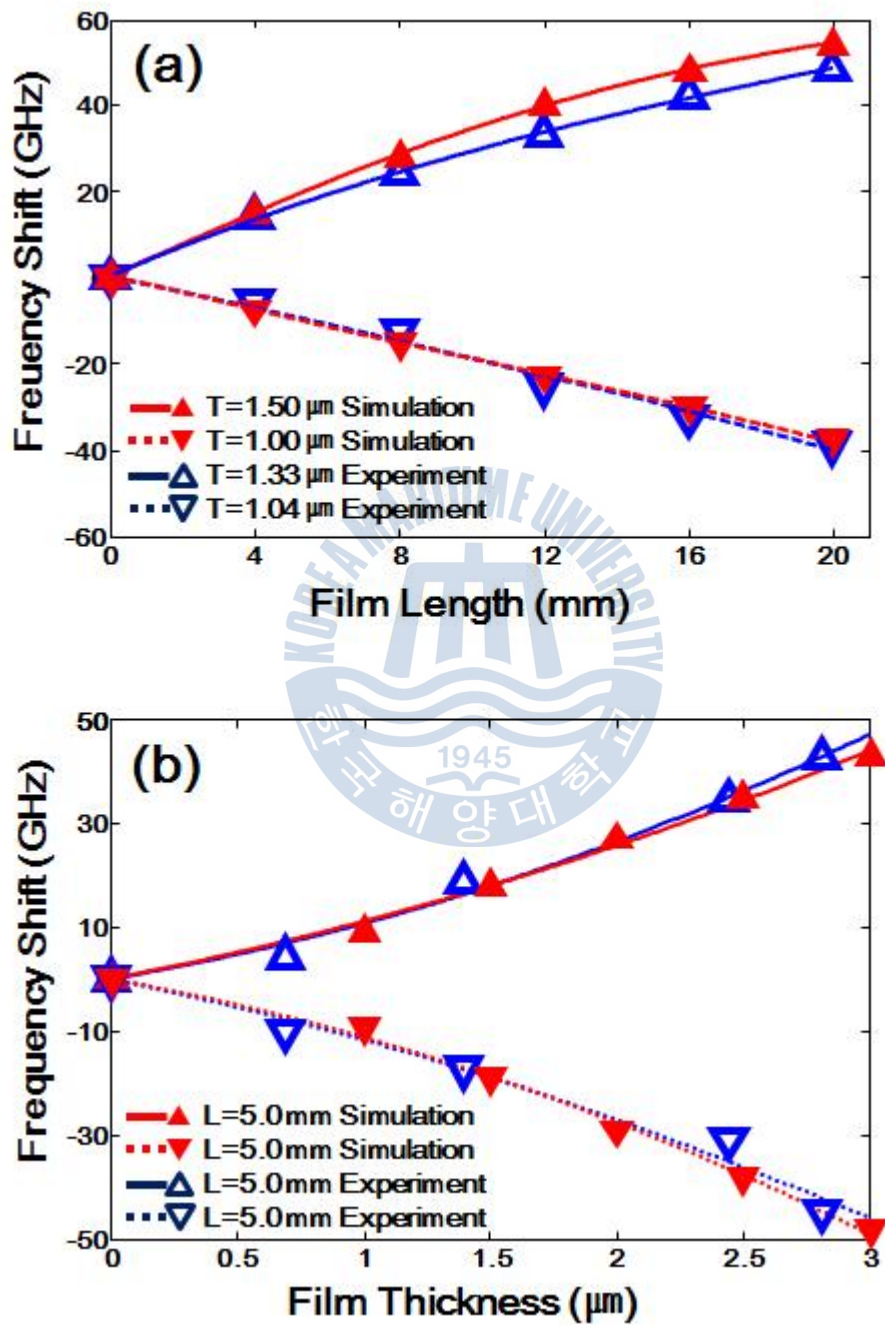


Fig. 4.17. Comparison of the experimental (blue) and simulated (red). The solid and dashed lines indicate linear fitting for the data. **(a)** Frequency shifts for different layer lengths. thin film thicknesses used in experimental and simulation conditions are 1.33 ± 0.18 and $1.50 \mu\text{m}$, respectively, for the open upper channel (red triangles) and 1.04 ± 0.08 and $1.00 \mu\text{m}$, respectively, for the open lower channel (inverse blue triangles). **(b)** Frequency shifts for different thin film thickness. Layer lengths used in experimental and simulation conditions are both 5 mm for the open upper channel (red triangles) and for the open lower channel (inverse blue triangles).

All experiment and FDTD simulation of results agree well. Experiment and FDTD simulation difference is allowed under understanding range of error from experiment. **Fig 4.17 (a)** experiment, which only open upper channel to measure dependent-length, is done with $1.33 \mu\text{m}$ thickness of thin film. But FDTD simulation is done $1.5 \mu\text{m}$. Our spin coating system has limitation to make accurate $1.5 \mu\text{m}$ thickness of thin film. Simulation has limitation (explained **Chater 4.4.1** simulation condition) too. Comparison experiment and simulation result has different condition of thin film. But, **Fig 4.17 (a)** show us only open lower channel FDTD simulation and experiment has similar thickness. two result is agreement.

Dependent-thickness experiment has problems like before experiment. **Fig 4.17 (b)** has FDTD simulation and experiment resonance shift. even though each experiment and FDTD simulation have different thickness of film. But, fitting line (upper and lower) show us good agreement.

4.4.5 Analysis

1) Time delay

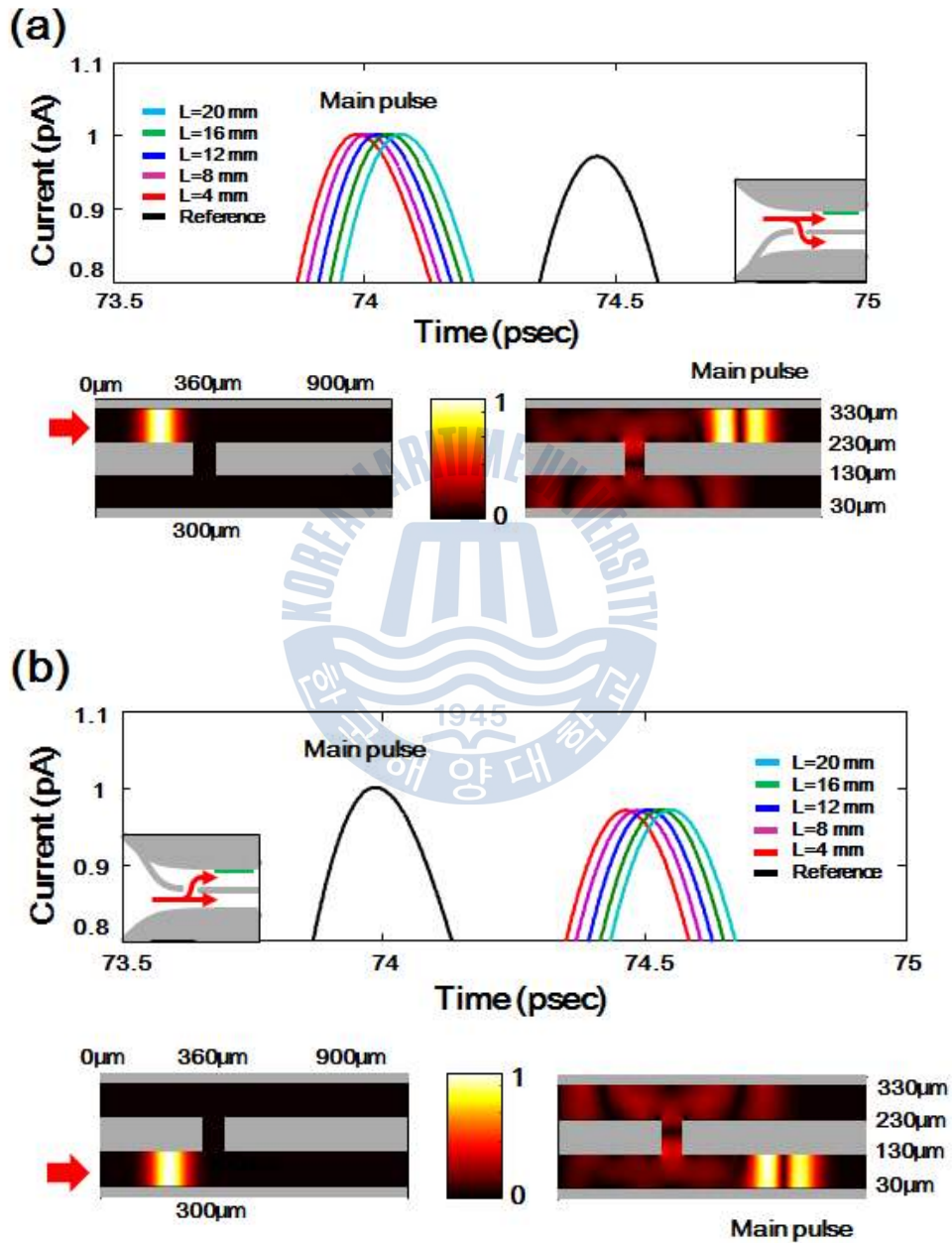


Fig. 4.18 2D FDTD simulation time domain shift and FDTD animation
(a) Main pulse and leak out of slit have time difference when input THz pulse travels to the upper channel only, (b) main pulse and leak out of slit have time difference when the input THz pulse travels to the lower channel only.

FDTD simulation can do newly analysis of the experiment in order to know principal of the resonance shift from PPWG sensing. **Fig 4.18** show us relation with resonance shift and time delay. only open one side of channel divide two pulse as single slit. 2D FDTD animation visually show us dividing pulse very well.

Detecting line in 2D FDTD divide two respectively. **Fig 4.18 (a)** only open upper channel show us dividing pulses. Main pulse propagate upper channel and meet with thin film. THz has a lot of interaction with thin film. So, main pulse delayed depend on film length. Leak out of slit pulse has longer way than main pulse which is input channel of pulse. But leak out of slit pulse has no thin film. that mean no delay. Two pulse time domain difference depend on thin film length is going to shorter than before when thin film length is longer than before. Two pulse time difference make resonance. So, time difference is decrease and resonance is shifting to high frequency.

Fig 4.18 (b) only open lower channel show us main pulse and leak out of slit pulse. Leak out of slit pulse propagate upper channel and meet with thin film. leak out of slit pulse delayed depend on characteristic of film. Main pulse has shorter way than leak out of slit pulse. But main pulse way has no thin film that mean no delay. Two pulse time domain difference depend on thin film length is going to longer than before when thin film length is longer than before. Two pulse time difference is making resonance. When time difference is increase, resonance is shifting to low frequency.

Our experiment detect sum of th both channel signal by using Si lens. Resonance shift comes out depend on thin film length as well as thickness, refractive index.

2) Phase Difference

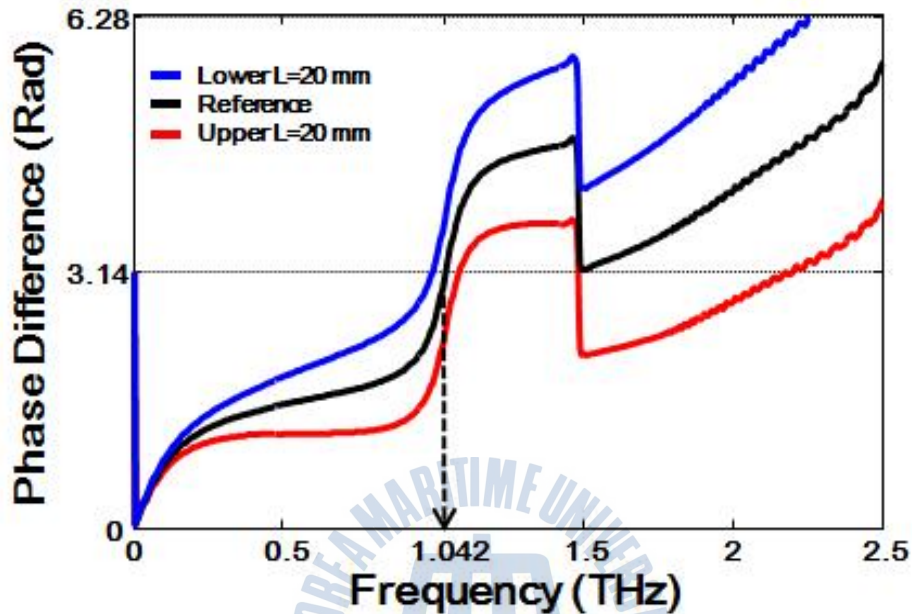


Fig. 4.19 Measured transmission spectra for different thin film lengths. Blue line is the input THz pulse travels to the upper channel only with 20 mm length of thin film. Red line is the input THz pulse travels to lower channel only with 20 mm length of thin film. black line is Reference (without thin film on PPWG).

Spectra and phase information come from time domain pulse. Phase information plot on the MATLAB program by using `unwrap(P)`, which is one of function : unwraps radian phases P by changing absolute jumps greater than or equal to π to their $2 \times \pi$ complement. Between reference and signal phase difference show us Fig 4.14. resonance point has 180 angle [π is 3.14] difference. Dot line arrow exactly indicate reference frequency. It mean two pulse wave cancel out at 180 angle.

3) High Q- factor resonance

The quality factor or Q factor [18] is a characterizes a resonator's bandwidth relative to its center frequency. Fig 4.19 is calculated experiment data.

Table 4.8 Q-factor

channel	Length	Unit (μm)		Bandwidth	Q-factor
		Left	Rigth		
up	0	0.974	1.020	0.0459	31.43
	4	0.986	1.039	0.0529	27.27
	8	1.000	1.047	0.0470	30.69
	12	1.017	1.048	0.0310	46.54
	16	1.018	1.069	0.0510	28.29
down	20	1.010	1.092	0.0820	17.59
	0	0.993	1.056	0.0633	22.79
	4	0.994	1.044	0.0501	28.79
	8	0.991	1.033	0.0421	34.27
	12	0.977	1.021	0.0439	32.86
	16	0.962	1.018	0.0559	25.81
	20	0.945	1.017	0.0717	20.12

Refractive index 1.7, Thickness 1.0 μm , depend on length

Table 4.8 show only open upper channel and lower channel each resonance bandwidth at -3dB. Only open upper channel has average 30.30 Q-factor. Only open lower channel has average 27.44 Q-factor. Some of Q-factor is higher or lowerer than others. Errors can understand under experiment errors. Also, this paper measurement have Q-factor resonator compare with other high Q-factor resonance. all experiment data have high Q-factor. Dependent length experiment **Chapter 4.4.4** is used to calculate Q-factor. These has similar value compare with other high Q-factor reference.

Chapter 5 Conclusion

5.1 Waveguide guides sensing

In conclusion, this research demonstrates thin dielectric layer sensing using two-channel PPWG with a single slit sheet. PPWG sensing overcome thin layer detection of wavelength limitation and possible detachable thin layer sensing. To know resonance frequency can do predict refractive index of thin layer. After the experimental setup, the upper PPWG block can be easily moved to coat the PPWG block surface and then installed. Therefore, this experimental scheme can be easily adapted to industrial and scientific applications, such as semiconductor and biological [19-21] studies, as an independent sensor.



Reference

- 1 M. van Exter and D. Grischkowsky, "Optical and electronic properties of doped silicon from 0.1 to 2 THz," Appl. Phys. Lett. 56,1694-1696 (1990).
- 2 M. van Exter and D. Grischkowsky, "Carrier dynamics and holes in moderately doped silicon," Phys. Rev. B. 41,12140-12149 (1990).
- 3 Kiyomi Sakai, "Terahertz Optoelectronics"
- 4 J. S. Melinger, N. Laman, S. S. Harsha, and D. Grischkowsky, "Line narrowing of terahertz vibrational modes for organic thin polycrystalline films in a parallel plate waveguide," Appl. Phys. Lett. 89, 251110 (2006).
- 5 W. Withayachumnankul, J. F. O'Hara, W. Cao, I. Al-Naib, and W. Zhang, "Limitation in thin-film sensing with transmission-mode terahertz time-domain spectroscopy," Opt. Express 22, 972-986 (2014).
- 6 Constantine A. Valanis, "Advanced Engineering Electromagnetics"
- 7 KANE.S. YEE, "Numerical solution of initial boundary value problems involving maxwell's equations in isotropic media", IEEE Transactions on antennas and propagation.
- 8 Lecture notes by John Schneider.
- 9 Sang-Hoon Kim, Eui Su Lee, Young Bin Ji, and Tae-In Jeon*, "Improvement of THz coupling using a tapered parallel-plate waveguide", Opt Express 18, 1289-1295 (2013).
- 10 Eui Su Lee,¹ Sun-Goo Lee,² Chul-Sik Kee,^{2,3,4} and Tae-In Jeon^{1,3,*}, "Terahertz notch and low-pass filters based on band gaps properties by using metal slits in tapered parallel-plate waveguides", Opt Express 19, 14852-14859 (2013).

- 11 "A Review on Thin-film Sensing with Terahertz Waves John F. O'Hara · Withawat Withayachumnankul · Ibraheem Al-Naib", Springer Science+Business Media.
- 12 M. Theuer, R. Beigang, and D. Grischkowsky, "Highly sensitive terahertz measurement of layer thickness using a two-cylinder waveguide sensor", APPLIED PHYSICS LETTERS 97, 071106 (2010).
- 13 Michael Nagel, Peter Haring Bolivar, Martin Brucherseifer, Heinrich Kurz, Anja Bosserhoff, and Reinhard Büttner, "Integrated planar terahertz resonators for femtomolar sensitivity label-free detection of DNA hybridization", APPLIED OPTICS 41, (2002).
- 14 MNagel, F Richter, P Haring-Bolivar and H Kurz, "A functionalized THz sensor for marker-free DNA analysis", Phys. Med. Biol. 48, 3625–636 (2003).
- 15 Christian Debus and Peter Haring Bolivar, "Frequency selective surfaces for high sensitivity terahertz sensing", Appl. Phys. Lett. 91, 184102 (2007).
- 16 Hu Tao, Andrew C. Strikwerda, Mengkun Liu, Jessica P. Mondia, Evren Ekmekci, Kebin Fan, David L. Kaplan, Willie J. Padilla, Xin Zhang, Richard D. Averitt, and Fiorenzo G. Omenetto, "Performance enhancement of terahertz metamaterials on ultrathin substrates for sensing applications", Appl. Phys. Lett. 97, 261909 (2010).
- 17 Kyungjun Song and Pinaki Mazumder, *Fellow, IEEE*, "Active Terahertz Spoof Surface Plasmon Polariton Switch Comprising the Perfect Conductor Metamaterial", IEEE TRANSACTIONS ON ELECTRON DEVICES 56, (2009).
- 18 S. S. Harsha, N. Laman, and D. Grischkowsky, "High- Q terahertz Bragg resonances within a metal parallel plate waveguide," Appl. Phys.Lett. 94, 091118 (2009).
- 19 M Nagel, M Först and H Kurz, "THz biosensing devices: fundamentals and technology," J. Phys.: Condens. Matter 18, S601–S618 (2006).
- 20 Z. Xu and P. Mazumder, *Fellow, IEEE*, "Bio-Sensing by Mach-Zehnder Interferometer Comprising Doubly-Corrugated Spoofed Surface Plasmon Polariton (DC-SSPP) Waveguide," IEEE Transactions on terahertz science and technology, 2,460-466 (2012).

21

M Nagel, F Richter, P H.-Bol'ivar and H Kurz, "A functionalized THz sensor for marker-free DNA Analysis," Phys. Med. Biol. 48, 3625–3636 (2003).

